PLOS ONE

RESEARCH ARTICLE

Evaluation of deacetylase inhibition in metaplastic breast carcinoma using multiple derivations of preclinical models of a new patient-derived tumor

Tiffany C. Chang[1,2☯]*, Margarite D. Matossian[1,2☯], Steven Elliott[1,2], Hope E. Burks[1,2], Rachel A. Sabol[2], Deniz A. Ucar[3], Henri Wathieu[1,2], Jovanny Zabaleta[4], Luis De Valle[5], Sukhmani Gill[1], Elizabeth Martin[6], Adam I. Riker[7], Lucio Miele[3], Bruce A. Bunnell[2], Matthew E. Burow[1,2], Bridgette M. Collins-Burow[1]*

1 Department of Medicine, Section of Hematology/Oncology, Tulane University School of Medicine, New Orleans, Louisiana, United States of America, **2** Department of Pharmacology, Tulane University School of Medicine, New Orleans, Louisiana, United States of America, **3** Department of Genetics, Louisiana State University School of Medicine, New Orleans, Louisiana, United States of America, **4** Department of Pediatrics, Louisiana State University School of Medicine, New Orleans, Louisiana, United States of America, **5** Department of Pathology, Louisiana State University School of Medicine, New Orleans, Louisiana, United States of America, **6** Department of Agricultural Engineering, Louisiana State University, Baton Rouge, Louisiana, United States of America, **7** Department of Surgery, Louisiana State University School of Medicine, New Orleans, Louisiana, United States of America

☯ These authors contributed equally to this work.
* tchang10@tulane.edu (TCC); bcollin1@tulane.edu (BMCB)

Citation: Chang TC, Matossian MD, Elliott S, Burks HE, Sabol RA, Ucar DA, et al. (2020) Evaluation of deacetylase inhibition in metaplastic breast carcinoma using multiple derivations of preclinical models of a new patient-derived tumor. PLoS ONE 15(10): e0226464. https://doi.org/10.1371/journal.pone.0226464

Editor: Lu-Zhe Sun, University of Texas Health Science Center, UNITED STATES

Received: November 27, 2019

Accepted: September 15, 2020

Published: October 9, 2020

Data Availability Statement: All relevant data are within the paper and its Supporting Information files.

Funding: This work was supported by grants from National Institute of Health (NIH) (Grants No. R01-CA125806-04 (MEB), 1R15CA176496-01A1 (MEB) and R01-CA174785-A1 (BMC-B)). This work was also supported in part by U54 GM104940 from the National Institute of General Medical Sciences of the National Institutes of Health, which funds the

Abstract

Metaplastic breast carcinoma (MBC) is a clinically aggressive and rare subtype of breast cancer, with similar features to basal-like breast cancers. Due to rapid growth rates and characteristic heterogeneity, MBC is often unresponsive to standard chemotherapies; and novel targeted therapeutic discovery is urgently needed. Histone deacetylase inhibitors (DACi) suppress tumor growth and metastasis through regulation of the epithelial-to-mesenchymal transition axis in various cancers, including basal-like breast cancers. We utilized a new MBC patient-derived xenograft (PDX) to examine the effect of DACi therapy on MBC. Cell morphology, cell cycle-associated gene expressions, transwell migration, and metastasis were evaluated in patient-derived cells and tumors after treatment with romidepsin and panobinostat. Derivations of our PDX model, including cells, spheres, organoids, explants, and *in vivo* implanted tumors were treated. Finally, we tested the effects of combining DACi with approved chemotherapeutics on relative cell biomass. DACi significantly suppressed the total number of lung metastasis *in vivo* using our PDX model, suggesting a role for DACi in preventing circulating tumor cells from seeding distal tissue sites. These data were supported by our findings that DACi reduced cell migration, populations, and expression of mesenchymal-associated genes. While DACi treatment did affect cell cycle-regulating genes *in vitro*, tumor growth was not affected compared to controls. Importantly, gene expression results varied depending on the cellular or tumor system used, emphasizing the importance of using multiple derivations of cancer models in preclinical therapeutic discovery research. Furthermore, DACi sensitized and produced a synergistic effect with approved oncology

Louisiana Clinical and Translational Science Center. The content is solely the responsibility of the authors and does not necessarily represent the official views of the National Institutes of Health. The funders had no role in study design, data collection and analysis, decision to publish, or preparation of the manuscript.

Competing interests: The authors have declared that no competing interests exist.

therapeutics on inherently resistant MBC. This study introduced a role for DACi in suppressing the migratory and mesenchymal phenotype of MBC cells through regulation of the epithelial-mesenchymal transition axis and suppression of the CTC population. Preliminary evidence that DACi treatment in combination with MEK1/2 inhibitors exerts a synergistic effect on MBC cells was also demonstrated.

Introduction

Metaplastic breast carcinoma (MBC) is a rare breast cancer subtype, comprising 0.45–1% of all breast cancers. This malignancy is molecularly and histologically heterogeneous, expressing both epithelial and mesenchymal features [1, 2]; MBC is commonly classified as the triple negative breast cancer (TNBC) PAM50 subtype due to lack of expression of estrogen or progesterone receptors and amplification of the human epidermal growth factor 2 (HER2/Neu) receptor [3]. Poor clinical outcomes are often associated with this cancer diagnosis: the 5-year survival rates for MBC are 38%-78%, compared to 76–93% for invasive ductal carcinoma [4]. A defining feature of MBC is the rapid tumor growth rate; this aggressive clinical presentation contributes to the lower survival rates of patients with MBC compared to patients afflicted with other intraductal carcinomas [4, 5]. When compared to another breast cancer subtype that has limited therapeutic targets and high rates of metastasis and relapse, TNBC patients afflicted with MBC have worse disease-free survival and overall survival [6, 7]. Despite these differences, MBCs are therapeutically managed similarly to other invasive breast carcinomas, with surgical resection in combination with radiation and/or chemotherapy [8]. However, MBCs have a worse response to neoadjuvant systemic chemotherapy [9] regimens including doxorubicin and cyclophosphamide, or doxorubicin and 5-fluorouracil, in comparison to the overall response of these regimens to other invasive breast cancer subtypes [4, 8, 10]. The characteristic heterogeneity within MBC, exemplified by the diverse histologic subtypes of MBC, and the dramatically different response rates to chemotherapy of the subtypes [11], contribute to why this malignancy is difficult to manage therapeutically [2, 12]. These findings emphasize the urgent necessity to identify novel therapeutic strategies that are specifically designed to target the unique and heterogeneous nature of MBC.

Targeted therapies have emerged as a novel approach to treat MBCs, since most MBC cases do not respond to standard systemic chemotherapy regimens. Emerging studies aim to identify novel therapeutic targets for MBC. The MBC transcriptome is similar to the claudin-low spectrum of basal-like breast cancers [13], and next-generation sequencing of 20 MBC tumors that represented various histologic subtypes identified frequent, targetable abnormalities and candidate targets to pursue in MBC including *TP53*, *PIK3CA*, *MYC*, *MLL2*, *PTEN*, *CDN2A/B*, *CCND3*, *CCNE1*, *EGFR*, and *KDM6A* [14]. A separate study of 18 patients using next-generation sequencing further supports these findings, as genetic alterations in the *PIK3CA*, *PTEN* and *AKT1* genes were identified in 50% of MBC tumors and *TP53* mutations were found in 56% of tumors [15]. Another group found *PIK3CA* mutations in 9 of 19 (48%) MBC tumors [16], and a more recent study detected *PIK3CA* mutations in 13 of 57 (23%) MBC tumors [17]. Additional targets are being pursued: 14 of 20 MBC patients had EGFR positive tumors [18], and a high prevalence (39 of 40) of MBC tumors harboring ribosomal protein L39 mutations were found to be susceptible to nitric oxide synthase inhibitors, implicated as a novel therapeutic strategy for some MBC tumors [19].

Early phase clinical trials of targeted therapies in combination with standard chemotherapy regimens support a role for combination therapy in MBC management. The role of the *PIK3CA/AKT/mTOR* axis in MBC has been demonstrated through targeted mTOR inhibition by temsirolimus, in combination with doxorubicin and bevacizumab, to improve response of MBCs, including a complete response [20]. Another example of the potential of combination therapy in MBC is demonstrated by a case study in which a patient with metastatic MBC had a remarkable response to anti-programmed death-ligand 1 (PD-L1) therapy in combination with nab-paclitaxel [21]. Comprehensive profiling of metaplastic breast carcinomas (N = 72 samples) revealed a high frequency of PD-L1 overexpression, significantly higher than in other TNBC subtypes [17]. Furthermore, although MBC is often compared to TNBC subtypes, MBC has distinct therapeutic responses. This is exemplified in a study demonstrating poor MBC response rate to poly (ADP-ribose) polymerase inhibitor therapy, a targeted therapy with promising effects in TNBC treatment [22]. A consistent limitation with clinical trials in MBC is that due to the rarity of this malignancy, patient recruitment for larger scale studies and MBC representation in breast cancer research is lacking [10]. Together, these studies show the variability in MBC responses to both targeted and combination treatment and emphasize the importance of establishing more translational MBC models to examine drug effects on this breast cancer subtype.

In this study, we evaluated the potential therapeutic efficacy of histone deacetylase inhibitors (DACi) in MBC. Histone deacetylase enzymes mediate chromatin remodeling, leading to silencing of genes that classically function to suppress tumor growth, inhibit cell-cycle progression, and induce apoptosis in cancer [23]. Paradoxically, this silencing mechanism of action drives tumorigenesis and metastasis. DACi are categorized based on distinct pharmacologic structures: romidepsin (FK228) is a cyclic peptide natural product and a selective HDAC1 and HDAC2 inhibitor, while panobinostat (LBH589), a nonselective deacetylase inhibitor, is a cinnamic hydroxamic acid analog of M-carboxycinnamic acid bishydroxamate [24]. These DACi have been investigated as targeted therapies for select cancer types: romidepsin and vorinostat are approved to treat cutaneous T-cell lymphoma [25], belinostat is approved to treat peripheral T-cell lymphoma [26], and panobinostat is approved to treat multiple myeloma [27]. Additionally, DACi therapies are in various stages of clinical trials for other cancer types, either as single agent or in combination therapies [28]. Examples include the combination of the DACi abexinostat with pazopanib in advanced renal cell carcinoma [29], the DACi vorinostat in combination with bevacizumab in clear-cell renal cell carcinoma [30], and the DACi abexinostat in combination with doxorubicin in metastatic sarcoma [31]. Other tumor types in which DACi therapy is being investigated include lung, pancreatic, advanced colorectal and hepatocellular carcinoma, Hodgkin lymphoma, hematologic malignancies, and breast cancer [28].

DACi have emerged as an effective targeted therapy in breast carcinomas in preclinical studies [32], specifically in TNBC subtypes [33]. Our laboratory has extensively evaluated DACi in TNBC cells and tumors [34–36]; we observed different biologic effects on tumorigenesis and metastasis with pan-DAC inhibition compared to class-specific inhibitors [35]. We have previously shown that aggressive breast cancer subtypes, such as TNBCs [34–36], specifically claudin-low TNBCs [36], are susceptible to DACi. Treatment with romidepsin and panobinostat reversed the mesenchymal phenotype of TNBCs, in addition to suppressing tumorigenesis and metastasis [35], consistent with findings from other groups [33, 37]. Maintenance of a mesenchymal phenotype is important in TNBC biology; the process through which cells acquire these cellular characteristics, also known as the epithelial-to-mesenchymal transition (EMT), is one proposed mechanism that is integral in the initiation of metastasis. In EMT, luminal breast cancer cells lose epithelial characteristics (cytoskeletal rearrangement,

loss of epithelial markers) and gain mesenchymal features (invasiveness, formation of cellular protrusions, expression of mesenchymal markers). This alteration facilitates detachment of the cells from the primary tumor and intravasation into the vasculature, through which the cells migrate and seed distal tissue sites [36]. Some studies have described the acquisition of mesenchymal characteristics contributing to tumor-initiating capabilities of cancer cells and tumor development [38, 39].

The associations amongst EMT, metastasis, and chemotherapeutic resistance are not completely understood. Expression of EMT-associated genes was initially thought to drive epithelial stem cell properties and breast cancer metastasis [40–42]. Other hypotheses suggest that EMT is not required for metastasis [43] and that epithelial- and mesenchymal-like states are mediated by the tumor microenvironment [44]. Despite this lack of congruency, targeted therapies that reverse the mesenchymal phenotype of cancer cells have been shown to improve the sensitivity of tumors to cytotoxic effects of chemotherapeutic agents [43, 45, 46]. Our group has previously demonstrated a similar role for DACi in combination therapy to re-sensitize endocrine-resistant breast tumors to therapeutic agents [47]. DACi treatment sensitizes TNBC cells to both targeted and systemic chemotherapies, especially DNA-damaging agents [17, 48, 49]. For example, DACi induced BRCA1 expression in TNBC cells and exhibited synergistic lethality with poly-ADP-ribose polymerase (PARP) inhibitor and cisplatin [50]. Another study found the DACi suberoylanilide hydroxamic acid to enhance anti-tumor effects of the PARP inhibitor olaparib in TNBC cells [51]. In this manuscript we aim to evaluate the therapeutic efficacy of DACi on the mesenchymal and metastatic phenotype of MBC and determine synergistic cytotoxic effects of DACi on MBC cells in combination with other targeted therapeutics.

Patient-derived xenograft (PDX) models are more translational than immortalized cell line-derived models because they maintain features that are present in the original patient tumor [52, 53]. Because MBC is a rare malignancy, there are fewer available model systems to study this disease compared to other breast cancer subtypes; it is crucial to develop new PDX models for MBC. Our group has established and characterized a new PDX MBC model, TU-BcX-4IC. Evaluating therapeutic response on various aspects of a patient's tumor is crucial to comprehensively understanding the mechanism of action on the complex biological systems that comprise MBC tumors: the cell population, cell clusters in suspension, cells in interaction with the extracellular matrix both *in vitro* (using organoids) and *ex vivo* (using tumor explants), and the intact tumor *in vivo*. Emerging studies show different responses of targeted drugs on cell viability and gene expression in adherent conditions compared to cells plated in suspension conditions [54, 55] and *ex vivo* treatments [56]. We hypothesize that by evaluating drug effects more comprehensively in the laboratory setting using this systems-based approach, there will be an improvement in the translation of preclinical observations into clinical practice.

There are currently no preclinical nor clinical studies that evaluate the role of DACi in MBC, to our knowledge. In this study we demonstrate the effect of histone deacetylase inhibitors on the mesenchymal phenotype and metastatic potential in a new PDX model derived from a clinically aggressive and drug-resistant MBC.

Materials and methods

Reagents and cell lines utilized

Human TNBC cell line MDA-MB-231 (HTB-26) was obtained from the American Type Culture Collection (ATCC, Rockville, MD) and authenticated by short tandem repeat profiling from ATCC. Dulbecco's modified Eagle's medium and non-essential amino acids were purchased from Caisson Laboratories (Smithfield, UT). Minimum essential amino acids, sodium

pyruvate, antibiotic-antimycotic, insulin, TrypLE were purchased from Invitrogen (Carlsbad, CA). Dimethyl sulfoxide was purchased from Thermo Fischer Scientific. Fetal bovine serum was obtained from Gemini Bio-Products (West Sacramento, CA). Romidepsin was purchased from ApexBio (Cat No. 3515; Batch No. 2; Houston, TX). Panobinostat was generously provided by Novartis Pharmaceutical Inc. (East Hanover, NJ).

Adherent cell culture

Cells were grown in DMEM supplemented with 10% fetal bovine serum (FBS), insulin, non-essential amino acids, minimal essential amino acids, antibiotic-antimycotic, and sodium pyruvate at 37˚C in 5% CO2.

Patient-derived xenografts

The metaplastic breast tumor model, identified as TU-BcX-4IC, was derived from a mastectomy specimen of a 57-year-old white female with metaplastic breast carcinoma unresponsive to neoadjuvant adriamycin/cyclophosphamide therapy. The tumor was obtained from the surgical specimen just after mastectomy. The mastectomy specimen was confirmed pathologically as a TNBC subtype. The tumor was obtained in collaboration with the Louisiana Cancer Research Center Biospecimen Core, which obtains tumor specimens from local hospitals. TU-BcX-4IC was propagated in SCID/Beige mice (CB17.cg-PrkdcscidLystbg/Crl) obtained from Charles River. The implantation procedures were carried out under anesthesia using a mixture of 5% isoflurane and oxygen delivered by mask initially and 1% isoflurane to maintain anesthesia. Following anesthetization with inhaled isoflurane, the surgical site was properly cleaned and disinfected with antiseptic surgical prep solution (e.g., iodine) prior to surgery. The tumor specimen was sectioned into 5x5 mm pieces under sterile conditions and coated in Matrigel (Cat No. 354234, Fisher Scientific, Waltham, MA, USA) to promote tumor take. The incision was made in the hypogastric region, and two 125 mm^3 tumors were implanted orthotopically into the mammary fat pad of SCID/beige mice. The incision was closed with wound clips, which were removed after 7–10 days. Incisions were ensured to be clean, intact without excessive tension by wound clips, and without signs of infection (e.g., swelling, redness, heat). Incisions were checked daily to ensure appropriate healing. After surgery, all mice were observed at a minimum frequency of 1 time every 2 minutes until ambulatory or responsive to gentle manipulation. Mice were not returned to the animal room until fully recovered from anesthesia. Clinical criteria include ability to reach food and water, absence of lethargy or altered mental status, and ability to remain upright. After regaining consciousness, mice were monitored for an additional 20 minutes for visible signs of pain or distress. Physiological criteria include absence of respiratory distress or labored breathing. Behavioral criteria include squinted eyes, hunched posture, decreased activity, abnormal gait or movements, greasy-looking coat, aggressiveness, and writhing contractions in the flank area. If physiologic and behavioral changes indicative of pain or distress were evident, per IACUC protocol, euthanasia was performed using CO_2 followed by cervical dislocation. Local analgesia (e.g., meloxicam) was administered to all mice prior to the incision and post-surgery, as needed, based on evidence of pain or discomfort.

After the first initial passage, Matrigel was no longer used, to show that TU-BcX-4IC grew independently of Matrigel. Mice were given subcutaneous injections of Meloxicam (5 mg/kg) prior to surgery. To passage the tumor, TU-BcX-4IC was implanted bilaterally into mammary fat pads of female SCID/Beige mice under anesthesia with a mixture of isoflurane and oxygen. Tumor volume was measured biweekly using digital calipers.

Following all surgeries, mice were monitored bi-weekly for tumor recurrence, pain, and distress, based on the criteria described above, for up to 20 days to detect metastatic seeding. Once tumor volume reached 1000 mm^3 or the mice showed signs of pain or distress, mice were euthanized with CO_2 and cervical dislocation, and the tumors were harvested for subsequent passage. Necropsy was performed and the lungs and liver were formalin-fixed and paraffin-embedded to observe baseline metastases.

This study was carried out in strict accordance with the recommendations in the Guide for the Care and Use of Laboratory Animals of the National Institutes of Health. The protocol was approved by Tulane University's Institutional Animal Care and Use Committee (Protocol Number: 635). All mice were housed in specific pathogen-free facilities at Tulane University's Vivarium. Compatible mice were housed in groups no larger than 5 in a plastic cage with a wire bar lid, water bottle, and commercially-available laboratory diet approved by the Vivarium. Environmental enrichment was provided through group housing of compatible mice and paper nesting material. Single housing was limited to mice in the immediate post-surgical period. All procedures performed were in accordance with ethical standards. All surgery was performed under isoflurane and oxygen anesthesia, and all efforts were made to minimize suffering.

Establishment of TU-BCx-4IC cell line

TU-BcX-4IC cells were established from the original TU-BcX-4IC tumor explant, before implantation into mice for propagation. The TU-BcX-4IC tumor explant was derived from the same mastectomy specimen used to establish our PDX model. TU-BcX-4IC tumor was dissected and a small tumor explant was plated in a 10 cm dish with DMEM supplemented with 10% FBS (described above). Adherent cells generated from the plated tumor were propagated until the TU-BCx-4IC cell line was established.

Generation of cell line-derived spheres

MDA-MB-231 and TU-BCx-4IC cells were plated in suspension conditions in low-attachment 96-well plates (1,000 cells per well), with serum-free F12/DMEM (Sigma-Aldrich, Carlsbad, CA; Cat. No D6421) supplemented with B-27 (ThermoFisher Scientific, Plaquemine, LA; Cat. No 17504044). Cells were maintained at 37˚C in humidified CO_2 for 24 hours to facilitate sphere formation. After 24 hours, suspended cells/spheres were treated with drug or DMSO controls every three days. Mammosphere growth was evaluated under brightfield microscopy (40X and 100X magnification) to quantify drug effects on sphere formation. The lengths and widths of individual spheres after treatments were measured using the Aperio ImageScope software. The area was calculated, recorded, and compared to DMSO treatment controls.

Crystal violet staining and dose/response quantification

The TU-BCx-4IC primary cell line established from the 4IC PDX tumor model, and MDA-MB-231 cells were utilized. Cells were maintained in DMEM supplemented with 10% FBS, insulin, non-essential amino acids, minimal essential amino acids, antibiotic-antimycotic, and sodium pyruvate at 37˚C in 5% CO_2. TU-BcX-4IC cells were exposed to charcoal-stripped media (phenol-free DMEM supplemented with 5% charcoal-stripped FBS (Gibco Invitrogen, Carlsbad CA), non-essential amino acids, minimal essential amino acids, Glutamax (Gibco Invitrogen, Carlsbad CA), penicillin-streptomycin (100 U/mL) for 24 hours. The following day, cells were treated with various concentrations of romidepsin, panobinostat, or DMSO treatment control. After three days, cells were fixed with glutaraldehyde and stained with crystal violet to observe the response to chemotherapies. Representative images were captured

with brightfield microscopy. The cells remaining were quantified by lysis with 33% acetic acid and absorbance was measured at 620 nm wavelength with a spectrophotometer.

Cell migration assays

TU-BcX-4IC cells were exposed to charcoal-stripped media (phenol-free DMEM supplemented with 5% charcoal-stripped FBS, non-essential amino acids, minimal essential amino acids, Glutamax, penicillin-streptomycin) for 24 hours. The following day, cells were treated with romidepsin (100 nM), panobinostat (100 nM), or DMSO treatment control (0.01% DMSO). After 48 hours of treatment, cells were counted using an automatic cell counter and 25,000 cells were plated on top of a migration chamber with 0.8-micron pores in serum-free Opti-MEM media (Gibco, USA). DMEM media (10% FBS) with supplements used for cell culture maintenance was plated in the bottom chamber. Cells were treated in-well for an additional 24 hours. Then, migration membranes were rinsed, scrubbed, fixed with formalin and stained with crystal violet. Membranes were mounted on slides and stained cells fixed to the membranes were quantified using the ImageJ software. Data is represented as mean ± standard error of the mean (SEM).

Confocal immunofluorescent visualization of cytoskeleton

To visualize the cytoskeleton, TU-BcX-4IC cells were incubated with Alexa Fluor® 555 Phalloidin (Cell Signaling Technology, Danvers, MA), which stains actin filaments. To detect and count nuclei, TU-BcX-4IC cells were incubated with DAPI (NucBlue Fixed Cell Stain ReadyProbe, Life Technologies, Carlsbad CA). ApoTome (commercial structure illumination microscopy by Zeiss, Thornwood, NY) fluorescent images were captured on an inverted microscope (Zeiss) and digitally filtered to obtain optical slices. Representative images were displayed to demonstrate changes in morphology in response to DACi treatment.

Generation of PDX-Os and live/dead fluorescence stain

When SCID/Beige mice implanted with TU-BcX-4IC tumors were passaged to maintain the tumor, small (2x2 mm^2) tumor pieces were plated in suspension culture conditions. Cells were allowed to grow out from the tumor pieces for 7 days, which contained mixed cell and stromal populations. At that time, PDX-Os were transferred to a 96-well ULA spheroid plate (Corning, NY, Cat. No. 4515) and treated with romidepsin or DMSO control. After 72 hours, media was removed and spheres were stained using the PromoKine live/dead staining kit (New York, USA). Cells were exposed to Calcein-AM (2μM) and Ethidium homodimer-III (5 μM) mixed with phosphate buffered saline. Calcein-AM can be transported through the cell membrane of live cells, where fluorescence activation is based on interaction with esterase enzymes. Ethidium homodimer binds to DNA of lysed (dead) cells. Cells were incubated for 45 minutes. Stained cells were imaged with confocal fluorescence microscopy and images were captured (8 images per well of adherent cells, 5 images per well of low-suspension cells). The 588 nM excitation channel was used to identify red, 'dead' cells, and the 420 nM excitation channel was used to visualize green, 'live' cells. Representative images were taken at 100x magnification.

RNA sequencing

After validating the integrity of the RNA samples in an Agilent BioAnalyzer 2100, 200 ng total RNA were used to make cDNA libraries using the TruSeq RNA Exome kit following the vendor's recommendations (Illumina) and sequenced at 2 x 75 bp in a NextSeq500 instrument (Illumina). FASTQ files were aligned to the *Homo sapiens*/hg19 reference genome using the

RNA-seq Alignment tool v1.1.1 in the Illumina's BaseSpace. Raw counts were extracted and used to find genes differentially expressed using DESEQ2 v1.16.1 in R-Studio 1.1.383. The data was normalized using the Variant Stabilizing Transformation and log2. A p value of <0.05 was considered significant and was further corrected by FDR < 0.05. Heatmaps were built using the *Pretty Heatmaps* application (pheatmaps) v1.0.10 in R-Studio.

Quantitative real time polymerase chain reaction

Total RNA was isolated and extracted from 4IC tumor samples and TU-BcX-4IC adherent cells using Quick-RNA MiniPrepTM (Zymo Research, Irvine, CA) according to manufacture protocol. After confirming RNA quality and quantity, RNA was reverse-transcribed (2 μg) into cDNA (iScript kit, BioRad Laboratories, Hercules, CA) and analyzed by qRT-PCR. Cycle number was normalized to β-actin and vehicle-treated cells scaled to 1, n = 3. Primers (Invitrogen, Carlsbad, CA) were generated with sequences as follows: *β-actin* F—5′- GGCACCCAG CACAATGAAGA-3′; *β-actin* R-5′- ACTCCTGCTTGCTGATCCAC -3′; *CDH1* F-5′-AG GTGACAGAGCCTCTGGATAGA-3′, *CDH1* R-3′-TGGATGACACAGCGTGAGAGA-3′; *VIM* F-5′-GAGAACTTTGCCGTTGAAGC -3′, *VIM* R-5′-GCTTCCTGTAGGTGGCAATC-3′; *CDH2* F-5′- GCCCCTCAAGTGTTACCTCAA -3′, *CDH2* R-5′-AGCCGAGTGATGGTCCA ATTT-3′; *ZEB1* F-5′- TGCACTGAGTGTGGAAAAGC-3′, *ZEB1* R-5′- TGGTGATGCT GAAAGAGACG-3′; *ZEB2* F-5′- CGCTTGACATCACTGAAGGA -3′, *ZEB2* R-5′- CTTG CCACACTCTGTGCATT-3′; *PLAU* F-5′- GGAAAACCTCATCCTACACAAGGA -3', *PLAU* R-5′- CGGATCTTCAGCAAGGCAAT-3′; *FOS* F-5′- GAATGCGACCAACCTTGTGC -3′, *FOS* R-5′- AGGGATCAGACAGAGGGTGT-3′; *FRA-1* F-5′- CGAAGGCCTTGTGAACAG AT-3′, *FRA-1 R*-5′- CTGCAGCCCAGATTTCTCA-3′.

Treatment of cells with National Cancer Institute-approved oncology drug set

For these experiments, TU-BcX-4IC primary cell line established from the 4IC PDX tumor model, and MDA-MB-231 cells were utilized. Cells were maintained in DMEM supplemented with 10% FBS, insulin, non-essential amino acids, minimal essential amino acids, antibiotic-antimycotic, and sodium pyruvate at 37˚C in 5% CO_2. TU-BcX-4IC cells were seeded in 96-well plates and treated with the commercially available NCI oncology drug panel (https://wiki.nci.nih.gov/display/NCIDTPdata/Compound+Sets). After three days, cells were fixed with glutaraldehyde and stained with crystal violet to observe the response to chemotherapies. Representative images were captured with brightfield microscopy. Stained cells were quantified two ways: 1) crystal violet-stained cells were lysed with 33% acetic acid and absorbance was measured at 620 nm wavelength with a spectrophotometer or 2) visible cells remaining after treatment were quantified using the ImageJ program. For the ImageJ quantification, images were captured at 100X using brightfield microscopy, and three images per 96-well plate were quantified for each treatment group. Debris were not included in the quantification.

Ex vivo treatment of PDX tumor pieces

TU-BcX-4IC was resected from mice after passages 2 and 6 (T2 and T6) and dissected into 5x5 mm^3 pieces. Tumor pieces were plated in 12-well plates with 10% FBS/DMEM media and treated with romidepsin (100 nM) or DMSO control (0.1%) for 72 hours. TU-BcX-4ICT2 tumors were treated in duplicate due to limited tissue availability and TU-BcX-4ICT6 tumors were treated in triplicate. PDX-Es were collected after 72 hours, and RNA was extracted using Qiazol Lysis Reagent (Cat No. 79306; Qiagen, Valencia, CA, USA) and dissection of the tumor

with scissors. Total RNA was isolated and cDNA was made as described above. mRNA was analyzed by qRT-PCR.

In vivo treatment of TU-BcX-4IC xenografts

Female SCID/Beige mice (n = 5/group) were inoculated with TU-BcX-4IC tumor implants (3x3 mm^3) in the mammary fat pads. For these studies, mice were treated with romidepsin (0.25 mg/kg) or DMSO vehicle control twice a day. This dose was generated from pharmacokinetic and pharmacodynamic data. Treatments were initiated immediately after tumor implantation (after 24 hours) due to the rapid growth rate and tumor take of this PDX model. After tumors reached 850 mm^3 in volume, mice were euthanized. Lungs and livers were harvested to examine metastasis, and peripheral blood was collected.

Immunohistochemistry staining

Tumor specimens, lungs, and livers were harvested at necropsy, and fixed in formalin. The samples were sent to our Department of Pathology at Tulane University where they were paraffin-embedded, sectioned and stained with hematoxylin and eosin (H & E). Lungs and liver sections were imaged using the Aperio Scanscope instrument (Aperio Technologies, Inc., Vista, CA, USA). Quantification of metastasis to the lungs and livers was achieved using ImageScope software (Aperio Technologies, Inc.). Livers, lungs, and tumor tissues were processed by the Department of Histology and Pathology at Tulane University. As per standard protocol, formalin-fixed tissues were paraffin-embedded, sectioned at 4 μM, and mounted on glass slides. Mounted sections were then exposed to xylene, ethanol, and acetic acid with intermittent washings with water before being stained with hematoxylin and eosin. After staining, slides were then again exposed to ethanol and xylene to complete the protocol.

Flow cytometry for cancer stem cell populations

Circulating tumor cells were collected in whole blood with 0.5M EDTA (Gibco Invitrogen, Carlsbad CA), incubated in red blood cell lysis buffer (0.008% NH4Cl, pH 7.2–7.4; Sigma-Aldrich, St. Louis MO), and washed with PBS. Collected cells from the tumor and blood samples were placed in staining solution containing 1% Bovine Serum Albumin (BSA; Sigma-Aldrich) and 1% CD16/CD32 Mouse BD Fc BlockTM (BD Biosciences) in PBS. The following primary antibodies were used: Anti-human CD24 (APC), and anti-human/mouse CD44 (PE-Fluor 610) purchased from eBiosciences (San Diego, CA, USA). All cells from the blood were analyzed with a Galios Flow Cytometer (Beckman Coulter, Brea, CA, USA) running Kaluza software (Beckman Coulter). At least 5000 events were analyzed and reported as the mean ± SEM.

Statistical analysis

The data was analyzed through unpaired Student's *t*-tests performed in Prism v7 (Graphpad, Inc.) with p-values < 0.05 considered statistically significant. Error bars are represented as mean ± standard error of mean (SEM). All dose-response and qRT-PCR performed in triplicates unless otherwise stated.

Results

DAC inhibition suppresses viability of TU-BcX-4IC cells in a dose-dependent manner and reverses mesenchymal morphology

To understand the role of histone DACi in metaplastic breast cancer, we first evaluated drug effects on cell viability and cell morphology of TU-BcX-4IC cells derived from an MBC patient

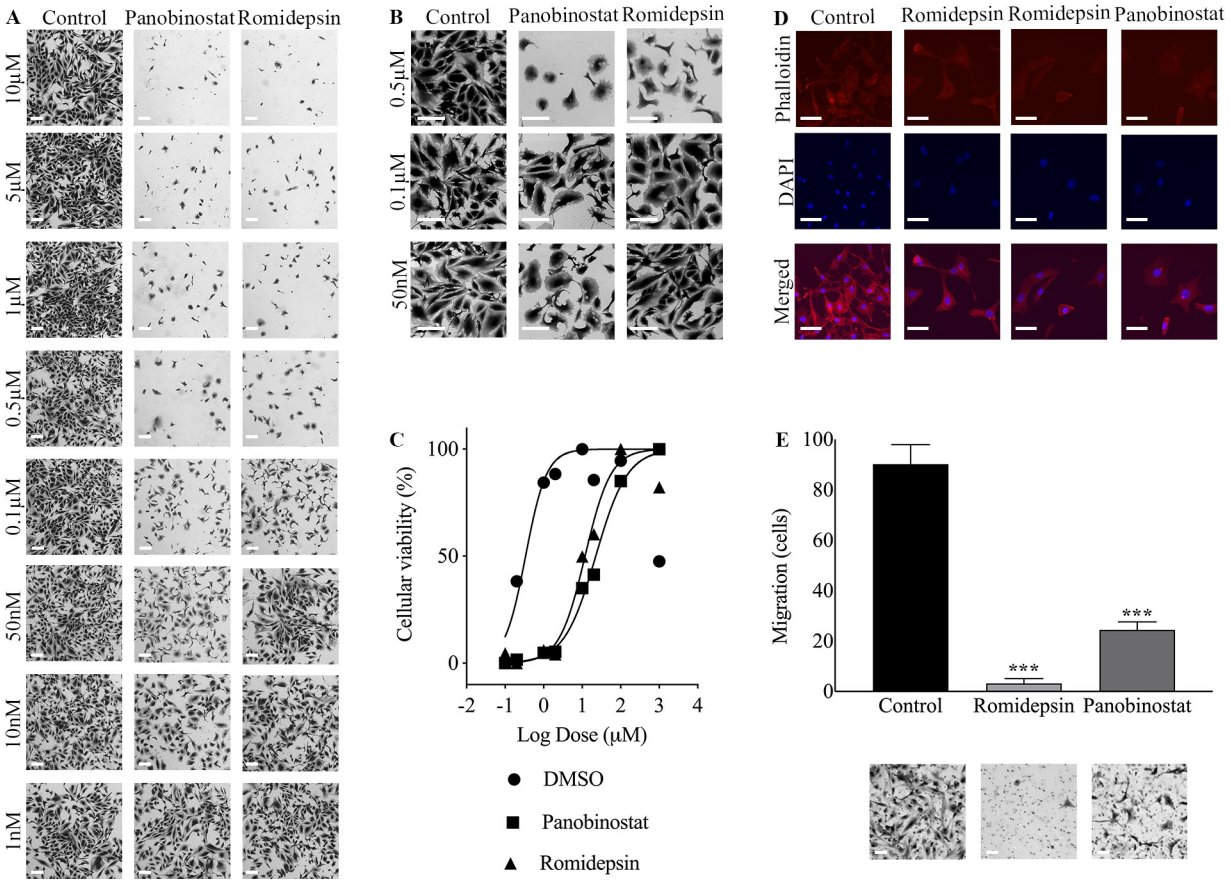

Fig 1. Dose-dependent response to panobinostat or romidepsin in adherent TU-BcX-4IC cells. TU-BcX-4IC cells were plated and treated with serial dilutions of panobinostat, romidepsin, or DMSO control for 72 hours. Cell viability and morphology were compared to DMSO control. Images were captured at 4X and 10X. (A) Panobinostat and romidepsin treatment to TU-BcX-4IC adherent cells demonstrate cytoxicity at 50 nM and 0.1 μM, respectively. Representative images are shown at 4X magnification. (B) Panobinostat and romidepsin treatment reverse the mesenchymal transition and promote epithelial-like characteristics. Representative images are higher magnifications of the samples in panel A; images are shown at 10X magnification. (C) Dose-response analysis of TU-BcX-4IC treated with panobinostat, romidepsin, or DMSO shows increased potency and efficacy of romidepsin compared to panobinostat. After crystal violet staining, plates were lysed and absorbance was measured (570 nm) and normalized to DMSO controls to quantify drug response. (D) TU-BcX-4IC cells stained with phalloidin and DAPI showed altered distribution of actin filaments in romidepsin, and panobinostat-treated cells. (E) Transwell migration of TU-BcX-4IC cells pre-treated for 72 hours with DMSO, romidepsin, or panobinostat (24 hours migration, 100 nM treatments). Error bars are represented as standard error of mean. $^{***}p < 0.001$. All scale bars represent 0.25 mm.

https://doi.org/10.1371/journal.pone.0226464.g001

tumor established in our laboratory. Cells were plated in adherent conditions and treated with panobinostat, romidepsin, or DMSO control for 72 hours. Cell viability was determined when crystal violet-stained cells were lysed, and absorbance was quantified. Both panobinostat and romidepsin reduced cell viability in dose-dependent manners, compared to DMSO control treatments (Fig 1A–1C). At 0.1 μM, there was sufficient inhibitor concentration to slow cellular growth, as evidenced by altered cellular morphology and decreased cellular viability. At higher inhibitor concentrations (e.g., 0.5 μM), cellular function and growth was disrupted to where the inhibitor exceeded the cellular capacity to respond to the offending agent, indicating cytotoxic levels of inhibitor. TU-BcX-4IC cells were more sensitive to panobinostat treatment, compared to romidepsin. IC50 values, calculated using nonlinear regressions with 4 parameters, were 22.56 μM (95% CI: 17.26 to 29.96 μM) for panobinostat and 11.90 μM (95% CI: 7.63 to 18.44 μM) for romidepsin. Major cytotoxic effects of DMSO alone were observed at final concentrations of 10 μM, or 1% DMSO, and greater. (Fig 1C). Alterations in cell morphology

were also observed in the DACi-treated cells. DAC inhibition reversed the mesenchymal cell morphology and increased epithelial features; the mesenchymal morphology is characteristic of the more metastatic TNBC subtypes. Suppression of the mesenchymal morphology is defined by fewer cells with protrusions, enhanced cell-cell contact, and rounder cell shapes [45]. To visualize the effects on DAC inhibition on cytoskeletal proteins, DMSO control, romidepsin, and panobinostat-treated cells were stained with phalloidin and DAPI to show actin filaments and nuclei, respectively. Microscopy showed reduced actin filaments and nuclei after DACi treatment (Fig 1D). Transwell migrations of cells treated for 72 hours with DMSO, romidepsin, and panobinostat showed decreased migration at 100 nM. Romidepsin treatment more significantly decreased cell migration, compared to panobinostat and the DMSO control (Fig 1E).

Patient-derived xenograft organoids (PDX-O) have emerged as a translational model to evaluate cytotoxicity because they recapitulate the microanatomy of patient tumors. These models facilitate testing drug effects on a more translational model, in which cells solely grown in suspension culture. Furthermore, organoids have been shown to more accurately predict clinical response to therapeutics, compared to cell line studies [57, 58]. We examined romidepsin effects in TU-BcX-4IC PDX-Os. PDX-Os were established from TU-BcX-4IC PDX tumor explants and maintained in suspension culture conditions. PDX-Os were treated with romidepsin (100 nM) or DMSO control for 72 hours and stained with a live/dead kit; fluorescence microscopy was used to visualize relative live and dead cell populations. Romidepsin treatment resulted in increased cytotoxicity of cells in the organoids compared to DMSO controls (Fig 2A). This experiment was performed in quadruplicate, and all treated PDX-Os are shown in Fig 2A.

DAC inhibition does not affect tumor growth but suppresses circulating tumor cell populations in vivo

To assess the effect of DACi on tumor formation, TU-BcX-4IC PDX explants were implanted in SCID/Beige mice and mice were intraperitoneally treated with romidepsin (0.25 mg/kg/day) or DMSO vehicle. Notably, at baseline, TU-BcX-4IC exhibits rapid tumor growth rates, compared to other TNBC models established by our group. No significant change in tumor growth was observed in romidepsin-treated tumors (194.0 ± 26.86 N = 14) compared to DMSO-treated control tumors (160.0 ± 20.07 N = 14) (Fig 2B). Tumors were excised, and mice were monitored for an additional 20 days to evaluate metastasis. Histopathologic analysis of excised tumors revealed cancer cells with pleomorphic nuclei, mitotic figures, and hyperchromaticity in both romidepsin and DMSO-treated mice (S1 Fig). After 20 days, mice were euthanized and peripheral blood was harvested to examine the effect of DACi on levels of cancer stem cells within the circulating tumor cell (CTC) populations. CTCs were identified as HLA^+ (a human-specific marker), and $CD44^+CD24^-$ cells indicate cancer stem cells [59]. We found a significantly reduced percentage of circulating tumor and stem cells in the peripheral blood of romidepsin-treated mice compared to DMSO-treated mice (Fig 2C, S2 Fig). While these data show that romidepsin does not affect tumor formation, romidepsin suppresses the cancer stem cell phenotype that drives metastasis.

Romidepsin treatment suppresses metastasis in TU-BcX-4IC

Given our findings that romidepsin suppresses CTC populations in peripheral blood, we next evaluated the effect of romidepsin on TU-BcX-4IC metastasis in immunocompromised mice. Notably, at baseline TU-BcX-4IC is a highly metastatic PDX model with lesions to both lungs and livers. Lungs and livers were harvested, formalin-fixed, paraffin-embedded and H & E-stained to visualize and quantify metastatic lesions. Romidepsin significantly reduced the number of metastatic lesions to the lungs (DMSO: 45.75 ± 13.98 N = 4, Romidepsin:

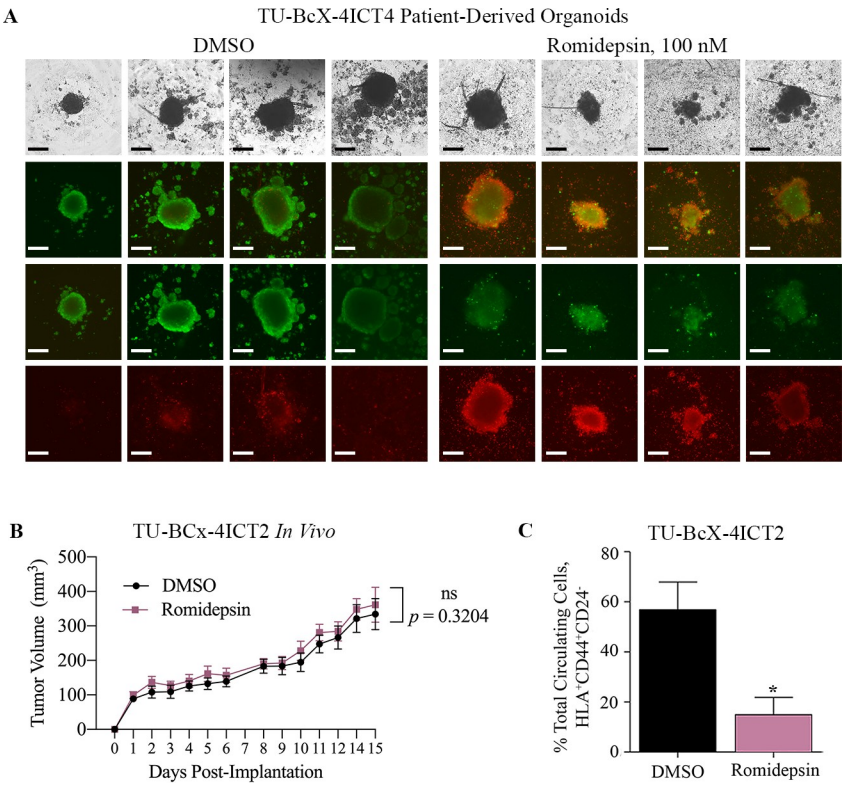

Fig 2. Romidepsin cytotoxicity to TU-BcX-4ICT4 patient-derived organoids and *in vivo* effects on tumorigenesis and circulating tumor cells. (A) PDX-Os were generated from TU-BcX-4ICT4 in 3D culture conditions and treated for 72 hours with romidepsin (100 nM) or DMSO control. PDX-Os were treated with a live (Calcein AM)/dead (EthD II) immunofluorescent staining kit to highlight live (green) or dead (red) cells. Representative images were captured at 40X magnification (brightfield images) or 50X magnification (immunofluorescent images). Scale bars represent 1.25 mm. (B) TU-BcX-4IC tumor pieces (passage 2; T2) were implanted bilaterally in the mammary fat pads of SCID/Beige mice treated with romidepsin or DMSO vehicle. Tumor volume was measured biweekly with calipers and after 20 days, tumors were excised and mice were sacrificed. (C) Twenty days after tumor excision, peripheral blood was collected to evaluate circulating tumor and stem cell populations, defined as $HLA^+CD44^+CD24^-$. Percentage of circulating tumor cells were significantly reduced in mice treated with romidepsin compared to those treated with DMSO. Error bars represent standard error of mean. $^*p < 0.05$.

https://doi.org/10.1371/journal.pone.0226464.g002

10.33 ± 2.028 N = 3) (Fig 3A), although the total area of lung metastatic lesions did not change significantly between the treatment and non-treatment groups (DMSO: 38930 ± 33090 N = 4, Romidepsin: 14920 ± 13180 N = 3) (Fig 3B). Although romidepsin reduced the total number and total area of liver metastases, neither the total number of metastatic lesions (DMSO: 26.00 ± 11.68 N = 3, Romidepsin: 15.00 ± 3.000 N = 3) (Fig 3D), nor the total area of metastases (DMSO: 887.8 ± 128.1 N = 3, Romidepsin: 776.8 ± 88.59 N = 3) (Fig 3E) were significantly reduced. Representative images of H & E-stained lungs (Fig 3C) and livers (Fig 3F) are included to demonstrate the size of metastatic lesions in the DMSO and romidepsin treatment groups. Together, these data show that although romidepsin treatment significantly decreased the number of lung metastases of the TU-BcX-4IC PDX model, no significant differences were observed in the total area of lung and liver metastasis.

Romidepsin suppresses EMT-associated genes in MBC

RNA-sequencing of TU-BcX-4IC cells treated with romidepsin or DMSO demonstrated that romidepsin affected the expression of genes involved with EMT, extracellular matrix, and cell

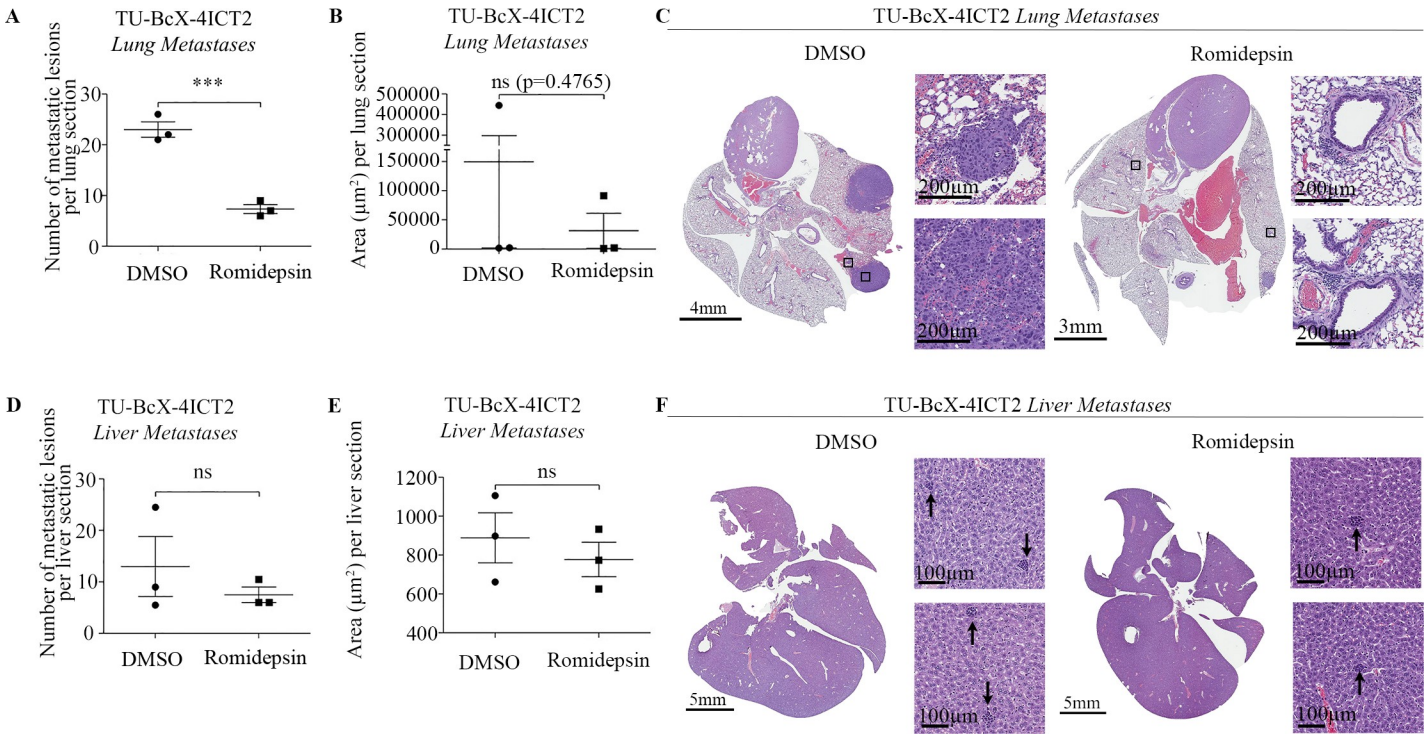

Fig 3. Romidepsin effect on metastasis in TU-BcX-4IC-implanted mice. Lungs and livers from mice implanted with TU-BcX-4IC and treated with romidepsin or DMSO vehicle were harvested, formalin-fixed, paraffin-embedded, and H&E-stained to visualize and quantify metastases. Romidepsin treatment (A) significantly decreased the number of metastatic lesions per lung section and (B) overall decreased the area of lung metastases compared to DMSO vehicle control. (C) Representative images of H&E-stained lungs in both treatment groups. The black box on the low magnification images indicates the regions shown in the higher magnification views. In liver sections, romidepsin (D) dramatically reduced the number of metastatic lesions per liver section and (E) overall decreased the area of liver metastases compared to DMSO, but these findings were not statistically significant. (F) Representative images of H&E-stained livers with arrows indicating metastatic foci in both treatment groups. Error bars represent standard error of mean (S.E.M.). $^{***}p < 0.0001$; ns = not significant.

https://doi.org/10.1371/journal.pone.0226464.g003

cycle signaling. In the EMT pathway, romidepsin interaction increased *CDH1*, *SNAI1* and *FOS* expression, and downregulated *VIM*, *CDH2*, *ZEB1*, *PLAU*, *JDP2*, *TGFB11*, *WNT5B*, *NFKB1*, *WNT5A*, *FOS*, *WNT3*, and *ZEB2* in addition to other mesenchymal genes (Fig 4A, S3 Fig). In cell cycle signaling pathways, romidepsin increased *CDNK1A* expression and downregulated *HDAC7*, *PLK1*, *AURKB*, *PLK4*, *CENPA*, *AURKA*, *MKI67*, and *FOXM1* (Fig 4B). Romidepsin also affected ECM-related genes including upregulation of *MMP9* and downregulation of *HAS2*, *PLAU*, *ADAMTS1*, *ECM2*, *ADAMTS5*, *DDR2*, *ADAM9*, *MMP14*, and *SERPINB1* (Fig 4C).

We have previously shown that DACi suppresses the mesenchymal genes *CDH2*, *VIM*, *ZEB1*, and *ZEB2*, and increases the epithelial gene *CDH1* in TNBC cells [34–36]. As mentioned previously, these genes were confirmed to be up- or downregulated in our RNA-sequencing analysis of TU-BcX-4IC cells treated with romidepsin compared to DMSO (Fig 4A). We used qRT-PCR with romidepsin or DMSO to examine if similar gene changes were observed in other *in vitro* derivations of an MBC PDX model: primary cell lines, spheres, and PDX-Os, and *in vivo* tumor implants (Fig 5A–5D, S4 Fig). Our data show that romidepsin significantly increases *CDH1* expression in the PDX-derived cell line, spheres, and PDX-Os. *CDH1* mRNA expression could not be observed in treated TU-BcX-4IC implanted tumors, due to low endogenous expression in the tumors. Across all studies, compared to DMSO, romidepsin significantly reduced expression of the mesenchymal gene *VIM*, although to a lesser degree in PDX-Os. *CDH2* expression was downregulated by romidepsin in tumor implants but not in

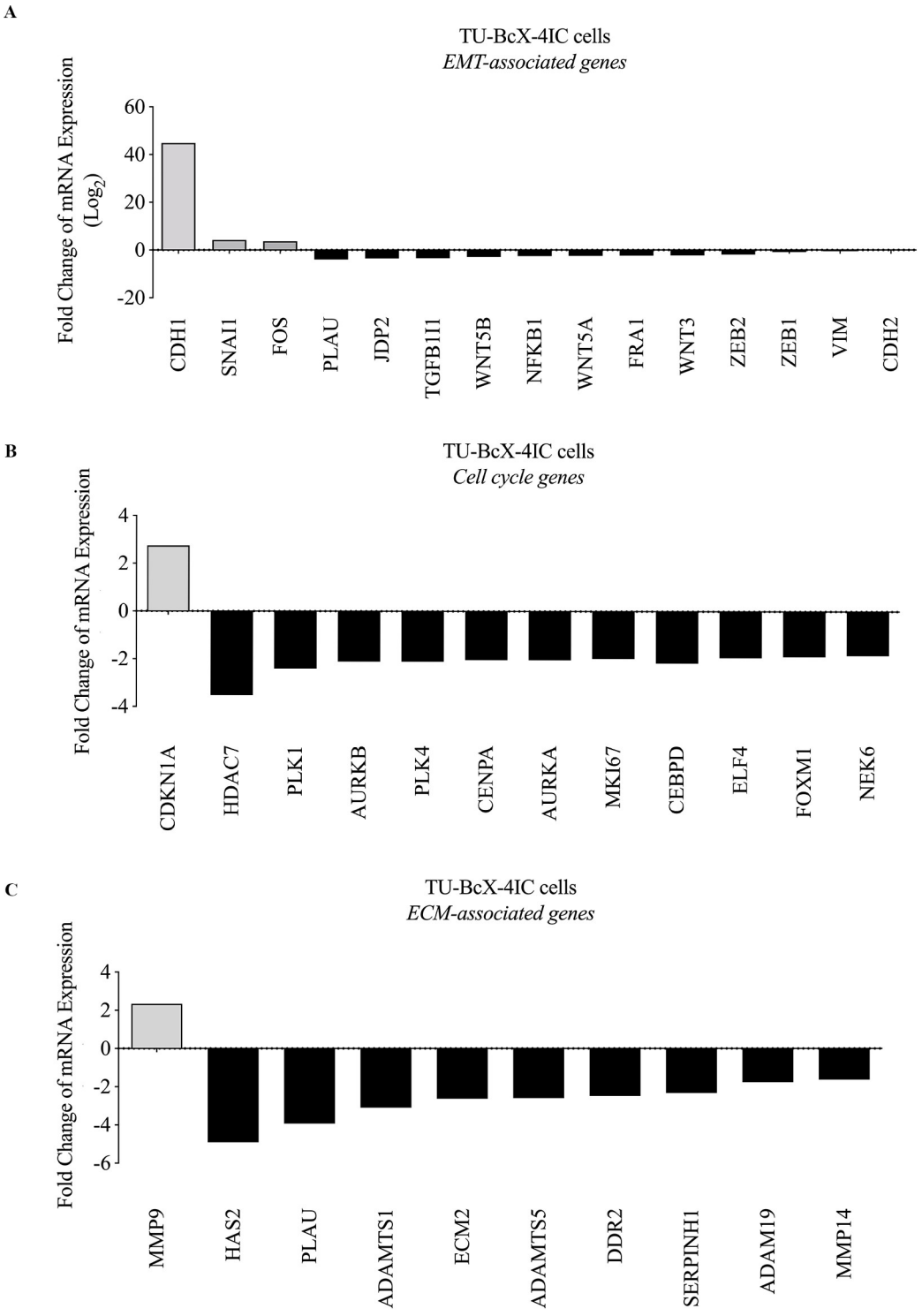

Fig 4. RNA sequencing analysis of romidepsin-treated TU-BcX-4IC cells compared to DMSO control. Romidepsin altered expressions of (A) EMT-related genes. Other cell signaling pathways that were affected include (B) cell cycle genes and (C) extracellular matrix-associated genes in TU-BcX-4IC cells. Data is shown as Log2 (fold change). mRNA expression of EMT genes (*CDH1*, *VIM*, *CDH2*, *ZEB1*, *ZEB2*) were analyzed using qRT-PCR.

https://doi.org/10.1371/journal.pone.0226464.g004

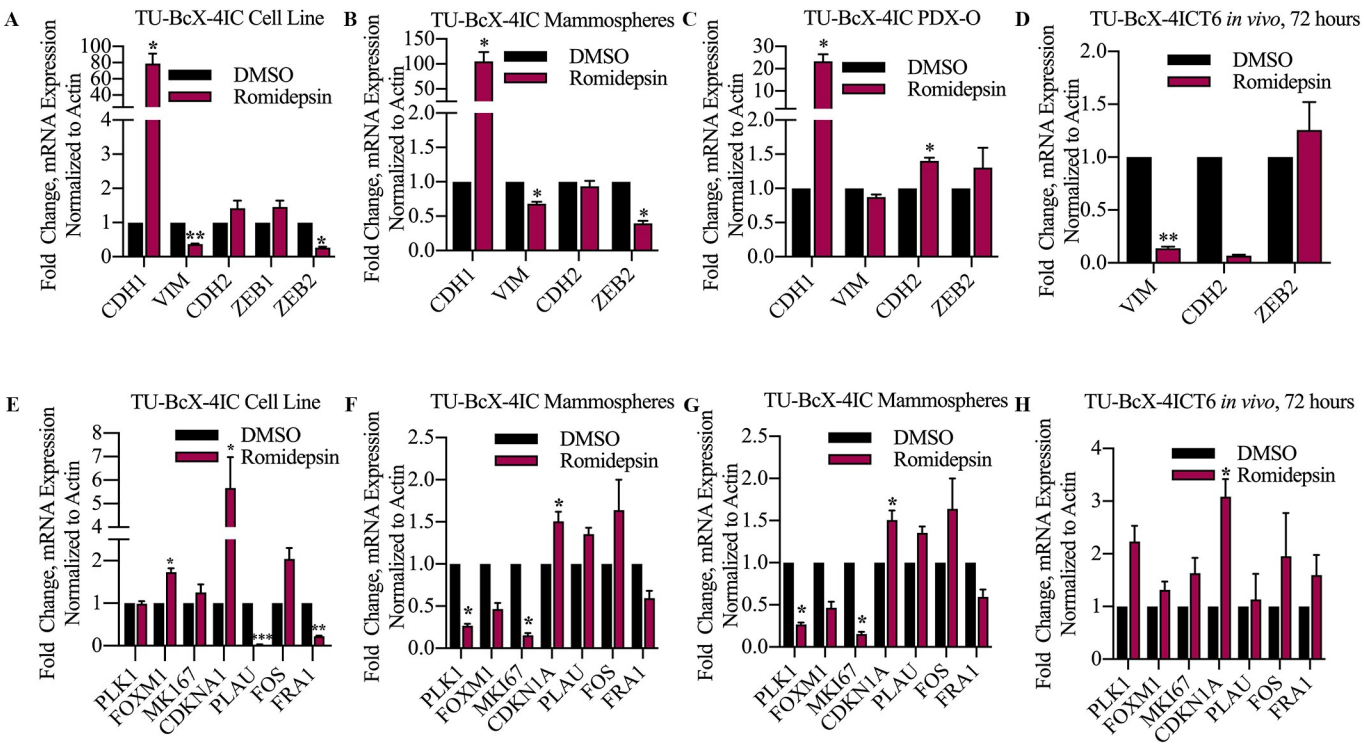

Fig 5. Effects of romidepsin on gene expression differs amongst treated cells, spheres, PDX-Os, and implanted tumors. Romidepsin treatment in TU-BcX-4IC (A) cell line, (B) spheres, (C) PDX-Os, and (D) *in vivo* tumor pieces implanted in SCID/Beige mice. qRT-PCR analysis was repeated with genes affected by romidepsin treatment compared to DMSO control based on RNA sequencing analyses (*PLK1*, *FOXM1*, *MKI67*, *CDKN1A*, *PLAU*, *FOS*, *FRA1*). Again, romidepsin-treated TU-BcX-4IC (E) cells, (F) spheres, (G) PDX-Os, and (H) *in vivo* tumor pieces implanted in mice were used. Analyses were all normalized to β-actin and DMSO treated controls. Black bars represent DMSO; maroon bars represent romidepsin treatment (100 nM, 72 hours). $^{*}p < 0.05$, $^{**}p < 0.01$, $^{***}p < 0.001$.

https://doi.org/10.1371/journal.pone.0226464.g005

cells. *ZEB1* expression was not altered after romidepsin treatment in cells; *ZEB1* expression could not be observed in treated TU-BcX-4IC spheres, PDX-Os, nor tumor implants due to low endogenous transcript levels. Interestingly, *ZEB2* expression was significantly downregulated in TU-BcX-4IC cells and spheres, although not in PDX-Os. This variability in gene expression suggests that other microenvironmental/stromal factors may play a role in the observed reversal of the mesenchymal phenotype caused by DACi.

Next, we examined changes in expression of additional EMT-, cell cycle-, and ECM-related genes that were significantly up- or downregulated in our sequencing analysis using the same derivations of the TU-BcX-4IC PDX model (Fig 5E–5H, S4 Fig). Of the cell cycle genes assessed, *CDKN1A* was significantly upregulated in romidepsin-treated TU-BcX-4IC cells, spheres, PDX-Os, and implanted tumors. The other cell cycle genes analyzed (*PLK1*, *FOXM1*, *MKI67*) were downregulated in romidepsin-treated spheres and PDX-Os but were not changed after romidepsin treatment of the cell line (*FOXM1* was increased in the cells) nor tumor implants. *PLAU* and *FRA1* were downregulated and while FOS was upregulated in the romidepsin-treated cells, consistent with the RNA-sequencing findings. However, *PLAU* expression was only also downregulated in PDX-Os, but not in implanted tumors nor in spheres. Conversely, *FOS* expression was also upregulated in romidepsin-treated spheres and implanted tumors, but not in PDX-Os (*FOS* has a similar level of reduction as *PLAU* in PDX-O). *FRA-1* expression was downregulated in romidepsin-treated spheres and PDX-Os but had increased expression in implanted tumors. These findings show the differences in

gene expression changes in cells compared to that in spheres, PDX-Os, and tumor implants; and thus, emphasize the importance of further analysis beyond the effects in monolayer cell populations in order to identify mechanisms of DACi on TNBC. In most derivations of our TU-BcX-4IC PDX model, romidepsin most consistently increased *CDH1* and *CDKN1A* gene expressions, and downregulated *VIM*, *ZEB2*, and *FRA1*.

Differences in DACi effects on gene expression in PDX-Es derived from various passages in mice and temporal variability in in vivo treated tumor implants

PDX explants (PDX-Es) are translational models, because they maintain the tumor microenvironment and architecture that is unique to each patient tumor. Next, we tested drug effects on intact tumor PDX-Es. To examine how treatment of different passage (T2 and T5) tumor PDX-Es potentially affects our interpretations of DACi in MBC, we treated various passage PDX-Es with romidepsin (100 nM) for 72 hours. We tested the EMT-associated genes described previously (*CDH1*, *VIM*, *CDH2*, *ZEB2*) and found that romidepsin increased *CDH1* expression in PDX-Es, while *VIM* and *ZEB2* expression was not affected by romidepsin in any passage of PDX-Es. *CDH1* expression was downregulated in PDX-E DMSO control groups. With respect to the RNA-seq identified genes (*PLK1*, *FOXM1*, *MKI67*, *CDKN1A*, *PLAU*, *FOS*, *FRA1*), we observed that overall, the cell cycle genes *PLK1*, *FOXM1*, and *MKI67* were consistently not altered after treatment of T2 nor T5 PDX-Es (only *FOXM1* expression was significantly upregulated). *CDKN1A* expression was upregulated late passage PDX-Es, but not in T2 PDX-Es. *PLAU* expression was downregulated in by romidepsin in T5 PDX-Es, but not in T2 (*PLAU* expression was upregulated instead). *FOS* was downregulated in T2 and upregulated in T5 PDX-Es treated with romidepsin. *FRA1* was downregulated in T2 and T5 PDX-Es. These data show inconsistencies with drug effects amongst treated intact tumor PDX-Es derived from various passages in mice.

Next, we sought to find short-term (72 hours) *in vivo* effects of romidepsin treatment on EMT gene expression in the tumors compared to a longer-term (15 days) *in vivo* treatment (S5A and S5B Fig). In both treatment groups, upregulation of *CDH1* expression was observed, with greater fold change in mRNA expression with short-term treatment (S5A Fig). These data, combined with the suppression of *VIM* and *CDH2* only in the short-term treatment group suggest changes in drug effectivity over time. These differences in gene expression were also observed between treatment groups for EMT-associated genes, cell cycle genes, and ECM-associated genes (S5C and S5D Fig). The EMT-associated gene *PLAU* was significantly downregulated in the long-term treatment group, compared to upregulation in the short-term treatment group. The EMT-associated gene *FRA1* was downregulated in both short- and long-term treatment groups, with significant downregulation in the long-term group (S5D Fig). The EMT-associated gene *FOS* and the cell cycle gene *FOXM1* were significantly upregulated in tumors treated with romidepsin for 15 days (S5D Fig), but not in those treated for 72 hours (S5C Fig). There was no significant difference between short- and long-term treatment groups for other cell-cycle genes (*PLK1*, *MK167*, *CDKN1A*). Together, these data identify EMT-associated and cell cycle gene expressions affected by the duration of DACi treatment in TU-BcX-4IC tumors *in vivo*.

Romidepsin pre-treatment sensitizes TU-BcX-4IC to NCI drugs

The link between EMT and drug sensitivity is an emerging area of research. Because we demonstrated that romidepsin suppresses the mesenchymal phenotype and thus, reverses EMT, we next evaluated if romidepsin sensitized TU-BcX-4IC cells to other targeted oncology agents.

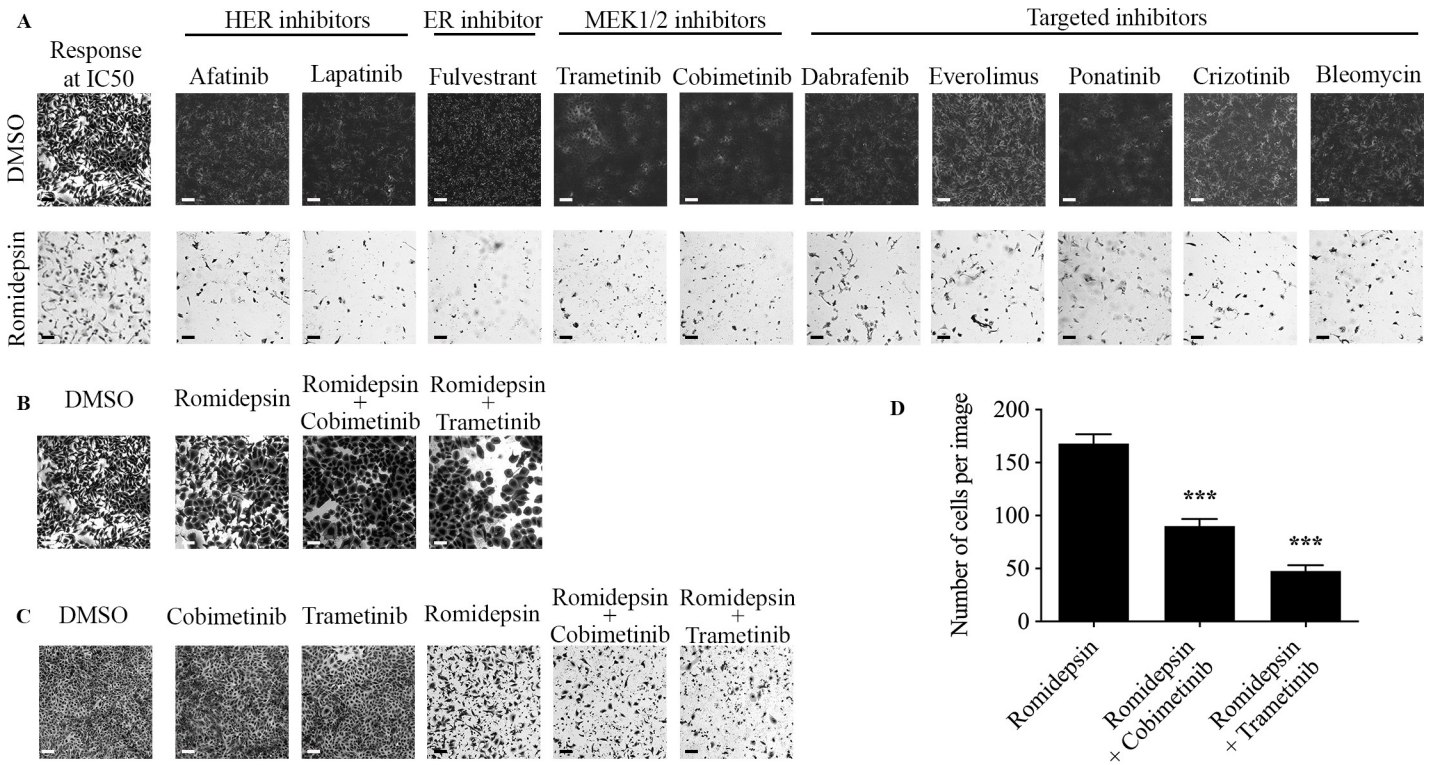

Fig 6. Romidepsin sensitizes TU-BcX-4IC cells to select oncology drugs. TU-BcX-4IC cells were treated only with agents from the NCI-approved oncology set or pre-treated with romidepsin (50 nM, 72 hours) prior to the oncology agents. Crystal violet staining was performed to visualize differences in cell viability between the groups. (A) Romidepsin sensitized TU-BcX-4IC cells to HER-targeted inhibitors (afatinib, lapatinib), the ER inhibitor fulvestrant, MEK1/2 inhibitors (trametinib, cobimetinib), as well as other targeted inhibitors (dabrafenib, everolimus, ponatinib, crizotinib), and bleomycin. Representative images are shown at 40X magnification. Response of both treatment groups to fluorouracil is shown as an example of baseline response to romidepsin, as well an example of 50% response of TU-BcX-4IC cells. (B) TU-BcX-4IC cells were pre-treated with romidepsin (50 nM) for 24 hours before treatment with cobimetinib and trametinib (1 μM) for an additional 24 hours. (C) TU-BcX-4IC cells were co-treated with romidepsin (50 nM) and cobimetinib or trametinib (1 μM) for 72 hours. (D) Quantification of cells remaining when cells were treated with romidepsin alone or pre-treated with romidepsin for 24 hours followed by cobimetinib or trametinib. Notably, the abundance of cells in the DMSO group prevented quantification of this treatment control and is not included in the graph. All scale bars represent 0.25 mm. $^{***}p < 0.001$.

https://doi.org/10.1371/journal.pone.0226464.g006

For these experiments, we used a set of clinically approved oncology drugs provided by the National Cancer Institute (NCI). We found TU-BcX-4IC cells to be inherently resistant to many of the drugs provided in the panel (Fig 6A). However, in an initial screen where we pre-treated TU-BcX-4IC cells with romidepsin (50 nM) resulted in markedly increased sensitivity to select drugs (Fig 6A). Pre-treatment with romidepsin increased sensitivity to HER-targeted inhibitors (afatinib, lapatinib), the estrogen-receptor inhibitor fulvestrant, and MEK1/2 inhibitors (trametinib, cobimetinib). Furthermore, pre-treatment increased sensitivity to other targeted inhibitors dabrafenib (BRAF), everolimus (mTOR), ponatinib (Bcr/Abl), crizotinib (c-MET, RON, ALK), and bleomycin (Fig 6A). Together, these data show that DACi adjuvant treatment sensitizes drug-resistant TU-BcX-4IC cells to clinically approved drugs. We also show drugs that were cytotoxic to both pre-treatment naive and romidepsin pre-treated cells, including bortezomib, mitoxantrone, topotecan, and epirubicin (S6 Fig). Then, we selected the two MEK1/2 inhibitors, cobimetinib and trametinib, that were sensitized with romidepsin-treated cells to further interrogate the effects of adjuvant romidepsin treatment. To confirm our findings that romidepsin sensitizes TNBC cells to MEK1/2 targeted therapy, we first replicated the initial screen by pre-treating TU-BcX-4IC cells with romidepsin for 24 hours before treating cells with cobimetinib and trametinib. TU-BcX-4IC cells pre-treated with romidepsin for 24 hours had increased sensitivity to the MEK1/2 inhibitors compared to romidepsin or

MEK1/2 inhibition alone (Fig 6B and 6D). Co-treatment (cells treated at the same time point) with romidepsin and cobimetinib or trametinib amplified a similar mesenchymal-to-epithelial transition phenotypic response that we observed in our initial morphology experiments (Fig 6C, S7 Fig). The TU-BcX-4IC cells appeared more epithelial morphologically: round-shaped cells with higher cytoplasm-to-nucleus ratios.

Discussion

Metaplastic breast cancer is a rare breast cancer subtype, for which there are limited therapeutic options. Clinically, MBCs exhibit rapid tumor growth rates and are chemo-refractory to a variety of chemotherapies [60]. There is a limited understanding of the underlying pathology and biological pathways that drive this proliferative tumor type, due to the rarity of MBC. Given the current treatment options with limited efficacy and poor response rates, insights into new therapeutic strategies or regimens for MBC are crucial. EMT is a proposed mechanism for the initiation of metastasis and acquisition of drug resistance in TNBC and MBC; pharmacologic inhibition of this transition is one proposed mechanism to prevent metastasis and resistance. We previously published that DACi reverses the mesenchymal morphology and mesenchymal gene expressions in aggressive TNBC subtypes [35, 36]. In this study, the response of MBC to DACi treatment was evaluated.

TU-BcX-4IC tumors implanted *in vivo* and TU-BcX-4IC patient-derived cells *in vitro* exhibit highly tumorigenic and metastatic capacities that model the clinically aggressive nature of MBC. Thus, this new PDX model is an ideal tool for studying drug effects on the dynamic processes that occur in resistant cancers. While DACi treatment in our MBC model suppressed some aspects of a mesenchymal cell phenotype, we did not observe the canonical EMT phenotypic change that we had previously observed with DACi treatment in other TNBC cells. Both inhibitors, panobinostat and romidepsin, were cytotoxic *in vitro* to TU-BcX-4IC cells and PDX-Os, and IC-50 concentrations differed with the DACis. Given the potential undesired side effects of using pan-DACi agents, in this study, we chose to focus on the response of TU-BcX-4IC to romidepsin, the targeted HDAC1/2 inhibitor. In previous studies, we found that romidepsin suppressed tumor growth and metastasis of established TNBC cell lines and implanted TNBC PDX tumors *in vivo* [34–36]. Romidepsin treatment did not significantly inhibit growth of TU-BcX-4IC implanted tumors in murine models, nor did treatment significantly reduce the average area of lung and liver metastases compared to DMSO control-treated tumors. Notably, romidepsin treatment significantly reduced number of lung metastases compared to vehicle control, suggesting that romidepsin prevents direct metastatic seeding to the lungs. The presence of cells that break free from the primary tumor and circulate before seeding in distal tissue sites has been investigated as a predictive measure for metastasis [61, 62]. It was also observed that romidepsin suppressed the number of circulating tumor cells (CTC) in the peripheral blood of mice implanted with TU-BcX-4IC tumors compared to vehicle control. Romidepsin treatment suppressed both MBC cell migration and mesenchymal gene expression. Together, these data support our working hypothesis that HDAC1/2 promotes lung tropism through regulation of the cells' capabilities to escape the primary tumor site and extravasate to the lungs. A limitation to our study was that one model was used; due to the rarity of this malignancy, testing DACi in other MBC PDX models are necessary to ascertain broader understanding of a role for DACi in MBC tumor growth and metastasis. Because our primary objective was to demonstrate overall pathways affected by DACi treatment in our MBC cell line and to compare *in vitro* approaches to testing drug response, future mechanistic studies are necessary to confirm specific gene expression changes due to romidepsin treatment in our MBC cell line, as well as other lines that represent the heterogeneity of TNBC.

This project was initiated to evaluate DACi therapy in MBC. Throughout the course of our experiments, we employed various derivations of PDX models to interrogate this objective. Profound observations were noted, which led us to pursue a secondary focus of this project: examining drug effects on different variations of PDX models. Depending on the cell or tumor system used, DACi had different effects on gene expressions. This resulted in contradictory conclusions pertaining to how DACi affected EMT and cell cycle genes in TNBC and MBC. These findings emphasized the importance of integrating multiple cell and tumor systems in drug discovery research, in order to draw more accurate conclusions regarding a drug's role in cancer. We compared DACi treatment in the patient-derived cell line, cells grown in suspension, PDX-Os, tumor pieces, and implanted intact tumors *in vivo*. We examined both EMT-related genes *(CDH1*, *VIM*, *ZEB1*, *ZEB2*, *CDH2*, *PLAU*, *FOS*, *FRA1)* [34, 35] and, since DACi regulates cell proliferation, cell cycle-related genes (*PLK1*, *FOXM1*, *CDKN1A*, *MKI67*). Patterns observed in genes consistently affected by all patient-derived models include *CDH1*, *VIM*, *FRA1*, and *CDKN1A*. Other genes were only affected in some models, including *ZEB2* which was downregulated in the cell line and spheres. These data demonstrate the response to romidepsin varied depending on the PDX-derived model used.

An interesting observation was that overall, gene expressions affected by romidepsin treatment in the 3D cultured spheres derived from the TU-BcX-4IC cell line were most similar to that of PDX-Os. Also, in the more translational models (PDX-Os, PDX-Es, and implanted tumors), there was reduced expression of *PLAU*, *FOS*, and *FRA1* in the implanted tumors compared to the PDX-Os and PDX-Es. Our findings are consistent with other groups that found drug sensitivity and associated gene expression changes differ in adherent compared to suspension culture systems, and *in vivo* analyses [55, 56, 63, 64]. One limitation in therapeutic discovery research is that laboratory findings are not often translated into clinical practice [65], and we believe integrating multiple derivations of PDX models is a step in overcoming this limitation.

We recognized difficulty in comparing drug effects on gene changes in tumors treated *in vivo*, which often occur in long time increments (15 days), to cells and tumor explants treated *in vivo* and *ex vivo* in shorter time increments (72 hours). To address this and to evaluate the temporal relationship between DACi treatment and its effects, we treated mice implanted with TU-BcX-4IC tumors for 72 hours *in vivo* and compared these findings to the long-term treatment group. While some genes remained unchanged, there were important differences, which support our hypothesis that romidepsin has both immediate and later-onset effects to suppress metastasis and alter downstream signaling pathways. Unique genes that were affected by short-term compared to longer-term treatments include upregulation of *CDKN1A* and suppression of *VIM* and *CDH2* expression. After long-term treatment, downregulation of genes for transcription factors (*FOS*, *ZEB1*, and *ZEB2)* and genes encoding proteins involved in cytoskeletal aspects of the mesenchymal morphology in EMT (*VIM* and *CDH2)* was observed. Because *VIM* and *CDH2* were more immediately downregulated compared to the transcription factors, combined with our findings that romidepsin promotes epithelial phenotypes after 72 hours, it can be inferred that romidepsin has an early effect on reversal of mesenchymal morphology. Then, romidepsin further suppresses metastatic effects after prolonged treatment by suppressing the transcription factors that drive the mesenchymal phenotype.

EMT has emerged as a potential mechanism of developing drug resistance in cancer [40, 45]; this is especially important in MBC due to de novo resistance to multiple cytotoxic therapies. Given our findings that DACi suppressed the mesenchymal phenotype, we investigated the role of DACi on chemoresistance using an NCI oncology drug set. TU-BcX-4IC cells were sensitized to various anti-cancer drugs including bleomycin, HER inhibitors afatinib and lapatinib, ER inhibitor fulvestrant, MEK1/2 inhibitors trametinib and cobimetinib, and other

targeted inhibitors (dabrafenib, everolimus, ponatinib, and crizotinib) following pre-treatment with romidepsin. These data suggest that DACi increases TU-BcX-4IC susceptibility to some oncology drugs. In addition, romidepsin improved TU-BcX-4IC cell sensitivity to bortezomib, mitoxantrone, topotecan, and epirubicin. The reversal of drug resistance after pre-treatment with romidepsin suggests preliminary evidence that DACis serve as additional therapeutic agents to current anti-tumorigenic drugs to maximize the therapeutic potential in highly resistant cancers. Two compounds were selected from the NCI drug panel set (cobimetinib and trametinib, MEK1/2 inhibitors) that, when combined with romidepsin, elicited a cytotoxic response to TU-BcX-4IC cells. These data implicate a synergistic role of DACi treatment with MEK1/2 inhibitors in MBC. This is consistent with previously published data regarding a synergistic role of DACi and MEK1/2 therapy in various tumor types. Some examples include the combined effects that induce fatality of leukemia cells [66], attenuate tumor growth of BRAF-mutated colorectal cells [67], and enhance the antitumor effects of MEK1/2 treatment in RAS-mutated lung cells [68].

In this study, we sought to evaluate DACi therapy in MBC using a new PDX model established by our group. When multiple derivations tumors and cells derived from the same PDX model were employed in mechanistic studies, the focus of the investigation shifted to emphasize the importance of using various cell and tumor systems to acquire a more complete and translational understanding of targeted drug response in complex breast cancer subtypes. Our findings are important in preclinical studies that evaluate the effects of novel therapeutic agents in all cancers and are not restricted to breast cancer. The application of multiple cancer models is necessary to more accurately translate preclinical observations into clinical practice.

Conclusions

The results of this study showed DACi suppression of migration and mesenchymal phenotypes in MBC, compared to DMSO controls. We demonstrated DACi regulation of the epithelial-mesenchymal transition axis and suppression of the CTC population. Our results serve as preliminary evidence that DACi treatment in combination with MEK1/2 inhibitors exerts a synergistic effect in MBC. Our results suggest that cancer models can serve as an important preclinical tool to identify effective therapeutic agents for complex breast cancer subtypes.

Supporting information

S1 Fig. Romidepsin cytotoxicity to tumors in patient-derived xenograft model. Tumors were excised, formalin-fixed, paraffin-embedded, and H & E-stained to visualize cellular composition and changes in romidepsin-treated tumors compared to DMSO control. Atypical histologic features were seen on both romidepsin and DMSO tumor specimens, including mitotic figures, nuclear pleomorphism, and hyperchromicity.
(TIF)

S2 Fig. Representative fluorescence activated cell sorting profile of circulating tumor cells in peripheral blood. Representative histogram of circulating tumor and stem cell populations, defined as $HLA^{+}CD44^{+}CD24^{-}$, in mice treated with (A) DMSO and (B) romidepsin were generated in Kaluza Analysis 2.1 Software (Beckman Coulter).
(TIF)

S3 Fig. Romidepsin modifies networks of EMT-related genes in TU-BcX-4IC cells compared to DMSO. Pathway analyses demonstrate the networks of EMT-related gene changes in romidepsin-treated TU-BcX-4IC cells compared to DMSO control treated cells. Data is shown as Log2 (fold change). Genes highlighted by green represent upregulated genes and

downregulated genes are highlighted in red.
(TIF)

S4 Fig. Romidepsin suppresses expression of EMT-associated genes and gene expression differs amongst treated cells, mammospheres, PDX-Os, PDX-Es, and implanted tumors. All data is shown as fold change ± SEM normalized to DMSO treatment controls.
(TIF)

S5 Fig. Effect of short-term treatment with romidepsin compared to long term effects on gene expression. Expression of EMT mRNAs (*CDH1*, *VIM*, *CDH2*, *ZEB1*, *ZEB2*) were analyzed using qRT-PCR. Romidepsin was evaluated in TU-BcX-4IC tumor pieces implanted in SCID/Beige mice. Drug effect studies were (A) short term (72 hours) or (B) long term (15 days). qRT-PCR analysis was repeated with genes affected by romidepsin treatment compared to DMSO control based on RNA sequencing analyses (*PLK1*, *FOXM1*, *MKI67*, *CDKN1A*, *PLAU*, *FOS*, *FRA-1*). Drug effect studies were (C) short term (72 hours) or (D) long term. Black bars represent DMSO; maroon bars represent romidepsin treatment (100 nM, 72 hours). All experiments were run in triplicate. Error bars are shown as S.E.M.
(TIF)

S6 Fig. TU-BcX-4IC cells were treated with oncology drugs selected from the NCI drug set cytotoxic to TU-BcX-4IC cells and compared to cells pre-treated with romidepsin. Crystal violet staining of TU-BcX-4IC cells pre-treated with romidepsin for 48 hours (50 nM), or without romidepsin, and then subsequently treated with the NCI oncology drug set. "FK" denotes FK228, or romidepsin, treatment. Scale bars represent 0.25 mm.
(TIF)

S7 Fig. Quantification of co-treatment studies with romidepsin and MEK 1/2 inhibitors (cobimetinib or trametinib) and pre-treatment studies with romidepsin. TU-BcX-4IC cells were concomitantly treated with romidepsin and a MEK 1/2 inhibitor. Pre-treatment with romidepsin was studied in TU-BcX-4IC cells by either pre-treating with romidepsin (50 nM) or not pre-treating for 48 hours, and then treating with cobimetinib or trametinib (1 μM). Crystal violet stained cells were lysed and absorbance was measured at 570 nm to quantify staining results.
(TIF)

Acknowledgments

Our group is very appreciative of the Genomics Core, under the direction of Dr. Erik Flemington, at Louisiana State University Health Sciences Center for performing the RNA sequencing. We also appreciate the collaboration with Alan Tucker in the Flow Cytometry and Cell Sorting Core Lab of Tulane Center for Stem Cell Research and Regenerative Medicine. We would also like to thank the Histology Core facilities at Tulane University for the hematoxylin and eosin stains of the tissue from the mice experiments. We would also like to thank the animal vivarium staff at Tulane University for their advice and assistance with the mice experiments. We are always grateful for the support, both financially and socially, of the Krewe de Pink organization in New Orleans. Finally, but most importantly, we are thankful to patients who donated their breast cancer tissue specimens to benefit breast cancer research; their contributions are valued and appreciated.

Author Contributions

Conceptualization: Matthew E. Burow.

Data curation: Steven Elliott, Adam I. Riker, Matthew E. Burow.

Formal analysis: Tiffany C. Chang, Margarite D. Matossian, Deniz A. Ucar.

Investigation: Tiffany C. Chang, Rachel A. Sabol, Deniz A. Ucar, Henri Wathieu, Jovanny Zabaleta, Luis De Valle, Elizabeth Martin, Lucio Miele, Matthew E. Burow.

Project administration: Margarite D. Matossian, Matthew E. Burow.

Supervision: Matthew E. Burow, Bridgette M. Collins-Burow.

Writing – original draft: Tiffany C. Chang, Margarite D. Matossian.

Writing – review & editing: Tiffany C. Chang, Margarite D. Matossian, Steven Elliott, Hope E. Burks, Rachel A. Sabol, Deniz A. Ucar, Henri Wathieu, Jovanny Zabaleta, Luis De Valle, Sukhmani Gill, Elizabeth Martin, Lucio Miele, Bruce A. Bunnell, Matthew E. Burow, Bridgette M. Collins-Burow.

References

1. Yamaguchi R, Horii R, Maeda I, Suga S, Makita M, Iwase T, et al. Clinicopathologic study of 53 metaplastic breast carcinomas: their elements and prognostic implications. Human pathology. 2010 May 1; 41(5):679–85. https://doi.org/10.1016/j.humpath.2009.10.009 PMID: 20153509
2. Tseng WH, Martinez SR. Metaplastic breast cancer: to radiate or not to radiate?. Annals of surgical oncology. 2011 Jan 1; 18(1):94–103. https://doi.org/10.1245/s10434-010-1198-6 PMID: 20585866
3. Alluri P, Newman LA. Basal-like and triple-negative breast cancers: searching for positives among many negatives. Surgical Oncology Clinics. 2014 Jul 1; 23(3):567–77. https://doi.org/10.1016/j.soc.2014.03.003 PMID: 24882351
4. Nelson RA, Guye ML, Luu T, Lai LL. Survival outcomes of metaplastic breast cancer patients: results from a US population-based analysis. Annals of surgical oncology. 2015 Jan 1; 22(1):24–31. https://doi.org/10.1245/s10434-014-3890-4 PMID: 25012264
5. Pezzi CM, Patel-Parekh L, Cole K, Franko J, Klimberg VS, Bland K. Characteristics and treatment of metaplastic breast cancer: analysis of 892 cases from the National Cancer Data Base. Annals of Surgical Oncology. 2007 Jan 1; 14(1):166–73. https://doi.org/10.1245/s10434-006-9124-7 PMID: 17066230
6. El Zein D, Hughes M, Kumar S, Peng X, Oyasiji T, Jabbour H, et al. Metaplastic carcinoma of the breast is more aggressive than triple-negative breast cancer: a study from a single institution and review of literature. Clinical breast cancer. 2017 Aug 1; 17(5):382–91. https://doi.org/10.1016/j.clbc.2017.04.009 PMID: 28529029
7. Ong CT, Thomas SM, Campbell BM, Greenup RA, Plichta JK, Rosenberger LH, et al. A population-based analysis of treatment and outcomes in 2,500 metaplastic breast cancer patients. 2017 May 30; 34 Suppl 15:532.
8. Rayson D, Adjei AA, Suman VJ, Wold LE, Ingle JN. Metaplastic breast cancer: prognosis and response to systemic therapy. Annals of Oncology. 1999 Apr 1; 10(4):413–9. https://doi.org/10.1023/a:1008329910362 PMID: 10370783
9. Al-Hilli Z, Choong G, Keeney MG, Visscher DW, Ingle JN, Goetz MP, et al. Metaplastic breast cancer has a poor response to neoadjuvant systemic therapy. Breast cancer research and treatment. 2019 Aug 1; 176(3):709–16. https://doi.org/10.1007/s10549-019-05264-2 PMID: 31119569
10. Shah DR, Tseng WH, Martinez SR. Treatment options for metaplastic breast cancer. ISRN oncology. 2012 Jun 21;2012.
11. Han M, Salamat A, Zhu L, Zhang H, Clark BZ, Dabbs DJ, et al. Metaplastic breast carcinoma: a clinicopathologic study of 97 cases with subset analysis of response to neoadjuvant chemotherapy. Modern Pathology. 2019 Feb 5; 32:807–16. https://doi.org/10.1038/s41379-019-0208-x PMID: 30723293
12. McCart Reed AE, Kalaw E, Nones K, Bettington M, Lim M, Bennett J, et al. Phenotypic and molecular dissection of metaplastic breast cancer and the prognostic implications. The Journal of Pathology. 2019 Feb; 247(2):214–27. https://doi.org/10.1002/path.5184 PMID: 30350370
13. Weigelt B, Kreike B, Reis-Filho JS. Metaplastic breast carcinomas are basal-like breast cancers: a genomic profiling analysis. Breast cancer research and treatment. 2009 Sep 1; 117(2):273–80. https://doi.org/10.1007/s10549-008-0197-9 PMID: 18815879
14. Ross JS, Badve S, Wang K, Sheehan CE, Boguniewicz AB, Otto GA, et al. Genomic profiling of advanced-stage, metaplastic breast carcinoma by next-generation sequencing reveals frequent,

targetable genomic abnormalities and potential new treatment options. Archives of Pathology and Laboratory Medicine. 2015 May; 139(5):642–9. https://doi.org/10.5858/arpa.2014-0200-OA PMID: 25927147

15. Zhai J, Giannini G, Ewalt MD, Zhang EY, Invernizzi M, Niland J, et al. Molecular characterization of metaplastic breast carcinoma via next-generation sequencing. Human pathology. 2019 Apr 1; 86:85–92. https://doi.org/10.1016/j.humpath.2018.11.023 PMID: 30537493

16. Hennessy BT, Gonzalez-Angulo AM, Stemke-Hale K, Gilcrease MZ, Krishnamurthy S, Lee JS, et al. Characterization of a naturally occurring breast cancer subset enriched in epithelial-to-mesenchymal transition and stem cell characteristics. Cancer research. 2009 May 15; 69(10):4116–24. https://doi.org/10.1158/0008-5472.CAN-08-3441 PMID: 19435916

17. Joneja U, Vranic S, Swensen J, Feldman R, Chen W, Kimbrough J, et al. Comprehensive profiling of metaplastic breast carcinomas reveals frequent overexpression of programmed death-ligand 1. Journal of clinical pathology. 2017 Mar 1; 70(3):255–9. https://doi.org/10.1136/jclinpath-2016-203874 PMID: 27531819

18. Leibl S, Moinfar F. Metaplastic breast carcinomas are negative for Her-2 but frequently express EGFR (Her-1): potential relevance to adjuvant treatment with EGFR tyrosine kinase inhibitors?. Journal of clinical pathology. 2005 Jul 1; 58(7):700–4. https://doi.org/10.1136/jcp.2004.025163 PMID: 15976335

19. Dave B, Gonzalez DD, Liu ZB, Li X, Wong H, Granados S, et al. Role of RPL39 in metaplastic breast cancer. JNCI: Journal of the National Cancer Institute. 2017 Jan 1; 109(6):djw292.

20. Basho RK, Gilcrease M, Murthy RK, Helgason T, Karp DD, Meric-Bernstam F, et al. Targeting the PI3K/AKT/mTOR pathway for the treatment of mesenchymal triple-negative breast cancer: evidence from a phase 1 trial of mTOR inhibition in combination with liposomal doxorubicin and bevacizumab. JAMA oncology. 2017 Apr 1; 3(4):509–15. https://doi.org/10.1001/jamaoncol.2016.5281 PMID: 27893038

21. Adams S. Dramatic response of metaplastic breast cancer to chemo-immunotherapy. NPJ breast cancer. 2017 Mar 29; 3(1):8.

22. Henneman L, van Miltenburg MH, Michalak EM, Braumuller TM, Jaspers JE, Drenth AP, et al. Selective resistance to the PARP inhibitor olaparib in a mouse model for BRCA1-deficient metaplastic breast cancer. Proceedings of the National Academy of Sciences. 2015 Jul 7; 112(27):8409–14.

23. Bolden JE, Peart MJ, Johnstone RW. Anticancer activities of histone deacetylase inhibitors. Nature reviews Drug discovery. 2006 Sep; 5(9):769. https://doi.org/10.1038/nrd2133 PMID: 16955068

24. Dokmanovic M, Clarke C, Marks PA. Histone deacetylase inhibitors: overview and perspectives. Molecular cancer research. 2007 Oct 1; 5(10):981–9. https://doi.org/10.1158/1541-7786.MCR-07-0324 PMID: 17951399

25. VanderMolen KM, McCulloch W, Pearce CJ, Oberlies NH. Romidepsin (Istodax, NSC 630176, FR901228, FK228, depsipeptide): a natural product recently approved for cutaneous T-cell lymphoma. The Journal of antibiotics. 2011 Aug; 64(8):525. https://doi.org/10.1038/ja.2011.35 PMID: 21587264

26. McDermott J, Jimeno A. Belinostat for the treatment of peripheral T-cell lymphomas. Drugs of today (Barcelona, Spain: 1998). 2014 May; 50(5):337–45.

27. Atadja P. Development of the pan-DAC inhibitor panobinostat (LBH589): successes and challenges. Cancer letters. 2009 Aug 8; 280(2):233–41. https://doi.org/10.1016/j.canlet.2009.02.019 PMID: 19344997

28. Li Y, Seto E. HDACs and HDAC inhibitors in cancer development and therapy. Cold Spring Harbor perspectives in medicine. 2016 Oct 1; 6(10):a026831. https://doi.org/10.1101/cshperspect.a026831 PMID: 27599530

29. Aggarwal R, Thomas S, Pawlowska N, Bartelink I, Grabowsky J, Jahan T, et al. Inhibiting histone deacetylase as a means to reverse resistance to angiogenesis inhibitors: phase I study of abexinostat plus pazopanib in advanced solid tumor malignancies. Journal of Clinical Oncology. 2017 Apr 10; 35 (11):1231. https://doi.org/10.1200/JCO.2016.70.5350 PMID: 28221861

30. Pili R, Liu G, Chintala S, Verheul H, Rehman S, Attwood K, et al. Combination of the histone deacetylase inhibitor vorinostat with bevacizumab in patients with clear-cell renal cell carcinoma: a multicentre, single-arm phase I/II clinical trial. British journal of cancer. 2017 Mar; 116(7):874. https://doi.org/10.1038/bjc.2017.33 PMID: 28222071

31. Choy E, Flamand Y, Balasubramanian S, Butrynski JE, Harmon DC, George S, et al. Phase 1 study of oral abexinostat, a histone deacetylase inhibitor, in combination with doxorubicin in patients with metastatic sarcoma. Cancer. 2015 Apr 15; 121(8):1223–30. https://doi.org/10.1002/cncr.29175 PMID: 25536954

32. Guerriero JL, Sotayo A, Ponichtera HE, Castrillon JA, Pourzia AL, Schad S, et al. Class IIa HDAC inhibition reduces breast tumours and metastases through anti-tumour macrophages. Nature. 2017 Mar; 543 (7645):428. https://doi.org/10.1038/nature21409 PMID: 28273064

33. Fedele P, Orlando L, Cinieri S. Targeting triple negative breast cancer with histone deacetylase inhibitors. Expert opinion on investigational drugs. 2017 Nov 2; 26(11):1199–206. https://doi.org/10.1080/13543784.2017.1386172 PMID: 28952409

34. Tate CR, Rhodes LV, Segar HC, Driver JL, Pounder FN, Burow ME, et al. Targeting triple-negative breast cancer cells with the histone deacetylase inhibitor panobinostat. Breast Cancer Research. 2012 Jun; 14(3):R79. https://doi.org/10.1186/bcr3192 PMID: 22613095

35. Rhodes LV, Tate CR, Segar HC, Burks HE, Phamduy TB, Hoang V, et al. Suppression of triple-negative breast cancer metastasis by pan-DAC inhibitor panobinostat via inhibition of ZEB family of EMT master regulators. Breast cancer research and treatment. 2014 Jun 1; 145(3):593–604. https://doi.org/10.1007/s10549-014-2979-6 PMID: 24810497

36. Matossian MD, Burks HE, Elliott S, Hoang VT, Bowles AC, Sabol RA, et al. Panobinostat suppresses the mesenchymal phenotype in a novel claudin-low triple negative patient-derived breast cancer model. Oncoscience. 2018 Mar; 5(3–4):99. https://doi.org/10.18632/oncoscience.412 PMID: 29854878

37. Garmpis N, Damaskos C, Garmpi A, Kalampokas E, Kalampokas T, Spartalis E, et al. Histone deacetylases as new therapeutic targets in triple-negative breast cancer: Progress and promises. Cancer Genomics-Proteomics. 2017 Sep 1; 14(5):299–313. https://doi.org/10.21873/cgp.20041 PMID: 28870998

38. Sikandar SS, Kuo AH, Kalisky T, Cai S, Zabala M, Hsieh RW, et al. Role of epithelial to mesenchymal transition associated genes in mammary gland regeneration and breast tumorigenesis. Nature communications. 2017 Nov 21; 8(1):1669. https://doi.org/10.1038/s41467-017-01666-2 PMID: 29162812

39. Anders CK, Carey LA. Biology, metastatic patterns, and treatment of patients with triple-negative breast cancer. Clinical breast cancer. 2009 Jun 1; 9:S73–81. https://doi.org/10.3816/CBC.2009.s.008 PMID: 19596646

40. Ye X, Tam WL, Shibue T, Kaygusuz Y, Reinhardt F, Eaton EN, et al. Distinct EMT programs control normal mammary stem cells and tumour-initiating cells. Nature. 2015 Sep; 525(7568):256. https://doi.org/10.1038/nature14897 PMID: 26331542

41. Ye X, Brabletz T, Kang Y, Longmore GD, Nieto MA, Stanger BZ, et al. Upholding a role for EMT in breast cancer metastasis. Nature. 2017 Jul; 547(7661):E1. https://doi.org/10.1038/nature22816 PMID: 28682326

42. Fischer KR, Durrans A, Lee S, Sheng J, Li F, Wong ST, et al. Epithelial-to-mesenchymal transition is not required for lung metastasis but contributes to chemoresistance. Nature. 2015 Nov; 527(7579):472. https://doi.org/10.1038/nature15748 PMID: 26560033

43. Liu S, Cong Y, Wang D, Sun Y, Deng L, Liu Y, et al. Breast cancer stem cells transition between epithelial and mesenchymal states reflective of their normal counterparts. Stem cell reports. 2014 Jan 14; 2(1):78–91. https://doi.org/10.1016/j.stemcr.2013.11.009 PMID: 24511467

44. Singh A, Settleman JE. EMT, cancer stem cells and drug resistance: an emerging axis of evil in the war on cancer. Oncogene. 2010 Aug; 29(34):4741. https://doi.org/10.1038/onc.2010.215 PMID: 20531305

45. Hennessy BT, Gonzalez-Angulo AM, Stemke-Hale K, Gilcrease MZ, Krishnamurthy S, Lee JS, et al. Characterization of a naturally occurring breast cancer subset enriched in epithelial-to-mesenchymal transition and stem cell characteristics. Cancer research. 2009 May 15; 69(10):4116–24. https://doi.org/10.1158/0008-5472.CAN-08-3441 PMID: 19435916

46. Shibue T, Weinberg RA. EMT, CSCs, and drug resistance: the mechanistic link and clinical implications. Nature reviews Clinical oncology. 2017 Oct; 14(10):611. https://doi.org/10.1038/nrclinonc.2017.44 PMID: 28397828

47. Mani SA, Guo W, Liao MJ, Eaton EN, Ayyanan A, Zhou AY, et al. The epithelial-mesenchymal transition generates cells with properties of stem cells. Cell. 2008 May 16; 133(4):704–15. https://doi.org/10.1016/j.cell.2008.03.027 PMID: 18485877

48. Ozaki KI, Kishikawa F, Tanaka M, Sakamoto T, Tanimura S, Kohno M. Histone deacetylase inhibitors enhance the chemosensitivity of tumor cells with cross-resistance to a wide range of DNA-damaging drugs. Cancer science. 2008 Feb; 99(2):376–84. https://doi.org/10.1111/j.1349-7006.2007.00669.x PMID: 18201278

49. Ono H, Sowa Y, Horinaka M, Iizumi Y, Watanabe M, Morita M, et al. The histone deacetylase inhibitor OBP-801 and eribulin synergistically inhibit the growth of triple-negative breast cancer cells with the suppression of survivin, Bcl-xL, and the MAPK pathway. Breast cancer research and treatment. 2018 Aug 1; 171(1):43–52. https://doi.org/10.1007/s10549-018-4815-x PMID: 29752686

50. Ha K, Fiskus W, Choi DS, Bhaskara S, Cerchietti L, Devaraj SG, et al. Histone deacetylase inhibitor treatment induces 'BRCAness' and synergistic lethality with PARP inhibitor and cisplatin against human triple negative breast cancer cells. Oncotarget. 2014 Jul; 5(14):5637. https://doi.org/10.18632/oncotarget.2154 PMID: 25026298

51. Min A, Im SA, Kim DK, Song SH, Kim HJ, Lee KH, et al. Histone deacetylase inhibitor, suberoylanilide hydroxamic acid (SAHA), enhances anti-tumor effects of the poly (ADP-ribose) polymerase (PARP) inhibitor olaparib in triple-negative breast cancer cells. Breast Cancer Research. 2015 Dec; 17(1):33.

52. Whittle JR, Lewis MT, Lindeman GJ, Visvader JE. Patient-derived xenograft models of breast cancer and their predictive power. Breast cancer research. 2015 Dec; 17(1):17.

53. Kawaguchi T, Foster BA, Young J, Takabe K. Current update of patient-derived xenograft model for translational breast cancer research. Journal of mammary gland biology and neoplasia. 2017 Jun 1; 22 (2):131–9. https://doi.org/10.1007/s10911-017-9378-7 PMID: 28451789

54. Friedrich J, Seidel C, Ebner R, Kunz-Schughart LA. Spheroid-based drug screen: considerations and practical approach. Nature protocols. 2009 Mar; 4(3):309. https://doi.org/10.1038/nprot.2008.226 PMID: 19214182

55. Edmondson R, Broglie JJ, Adcock AF, Yang L. Three-dimensional cell culture systems and their applications in drug discovery and cell-based biosensors. Assay and drug development technologies. 2014 May 1; 12(4):207–18. https://doi.org/10.1089/adt.2014.573 PMID: 24831787

56. Muraro MG, Muenst S, Mele V, Quagliata L, Iezzi G, Tzankov A, et al. Ex-vivo assessment of drug response on breast cancer primary tissue with preserved microenvironments. Oncoimmunology. 2017 Jul 3; 6(7):e1331798. https://doi.org/10.1080/2162402X.2017.1331798 PMID: 28811974

57. Abbasi J. Patient-derived organoids predict cancer treatment response. JAMA. 2018 Apr 10; 319 (14):1427.

58. Vlachogiannis G, Hedayat S, Vatsiou A, Jamin Y, Fernández-Mateos J, Khan K, et al. Patient-derived organoids model treatment response of metastatic gastrointestinal cancers. Science. 2018 Feb 23; 359 (6378):920–6. https://doi.org/10.1126/science.aao2774 PMID: 29472484

59. Sheridan C, Kishimoto H, Fuchs RK, Mehrotra S, Bhat-Nakshatri P, Turner CH, et al. CD44+/CD24- breast cancer cells exhibit enhanced invasive properties: an early step necessary for metastasis. Breast Cancer Research. 2006 Oct; 8(5):R59. https://doi.org/10.1186/bcr1610 PMID: 17062128

60. Hennessy BT, Giordano S, Broglio K, Duan Z, Trent J, Buchholz TA, et al. Biphasic metaplastic sarcomatoid carcinoma of the breast. Annals of Oncology. 2006 Feb 9; 17(4):605–13. https://doi.org/10.1093/annonc/mdl006 PMID: 16469754

61. Zhou L, Dicker DT, Matthew E, El-Deiry WS, Alpaugh RK. Circulating tumor cells: silent predictors of metastasis. F1000Research. 2017; 6.

62. Giuliano M, Giordano A, Jackson S, Hess KR, De Giorgi U, Mego M, et al. Circulating tumor cells as prognostic and predictive markers in metastatic breast cancer patients receiving first-line systemic treatment. Breast Cancer Research. 2011 Jun; 13(3):R67. https://doi.org/10.1186/bcr2907 PMID: 21699723

63. Riedl A, Schlederer M, Pudelko K, Stadler M, Walter S, Unterleuthner D, et al. Comparison of cancer cells in 2D vs 3D culture reveals differences in AKT–mTOR–S6K signaling and drug responses. J Cell Sci. 2017 Jan 1; 130(1):203–18. https://doi.org/10.1242/jcs.188102 PMID: 27663511

64. Breslin S, O'Driscoll L. The relevance of using 3D cell cultures, in addition to 2D monolayer cultures, when evaluating breast cancer drug sensitivity and resistance. Oncotarget. 2016 Jul 19; 7(29):45745. https://doi.org/10.18632/oncotarget.9935 PMID: 27304190

65. Kieburtz K, Olanow CW. Translational experimental therapeutics: The translation of laboratory-based discovery into disease-related therapy. Mount Sinai Journal of Medicine: A Journal of Translational and Personalized Medicine: A Journal of Translational and Personalized Medicine. 2007 Apr; 74(1):7–14.

66. Yu C, Dasmahapatra G, Dent P, Grant S. Synergistic interactions between MEK1/2 and histone deacetylase inhibitors in BCR/ABL+ human leukemia cells. Leukemia. 2005 Sep; 19(9):1579. https://doi.org/10.1038/sj.leu.2403868 PMID: 16015388

67. Carson R, Celtikci B, Fenning C, Javadi A, Crawford N, Perez-Carbonell L, et al. HDAC inhibition overcomes acute resistance to MEK inhibition in BRAF-mutant colorectal cancer by downregulation of c-FLIPL. Clinical cancer research. 2015 Jul 15; 21(14):3230–40. https://doi.org/10.1158/1078-0432.CCR-14-2701 PMID: 25813020

68. Yamada T, Amann JM, Tanimoto A, Taniguchi H, Shukuya T, Timmers C, et al. Histone deacetylase inhibition enhances the antitumor activity of a MEK inhibitor in lung cancer cells harboring RAS mutations. Molecular cancer therapeutics. 2018 Jan 1; 17(1):17–25. https://doi.org/10.1158/1535-7163.MCT-17-0146 PMID: 29079711